ESL-TR-87-73
VOL III

SCALING PROBLEMS FOR WAVE PROPAGATION IN LAYERED SYSTEMS VOLUME III

F.Y. SORRELL, Y. HORIE, J.K. WHITFIELD,
S.H. LEE, J.K. PARK

NORTH CAROLINA STATE UNIVERSITY
DEPARTMENT OF MECHANICAL & AEROSPACE ENGINEERING
RALEIGH NC 27695-7910

SEPTEMBER 1989

FINAL REPORT

MARCH 1985 — MARCH 1988

AIR FORCE ENGINEERING & SERVICES CENTER
ENGINEERING & SERVICES LABORATORY
TYNDALL AIR FORCE BASE, FLORIDA 32403

NOTICE

PLEASE DO NOT REQUEST COPIES OF THIS REPORT FROM HQ AFESC/RD (ENGINEERING AND SERVICES LABORATORY). ADDITIONAL COPIES MAY BE PURCHASED FROM:

NATIONAL TECHNICAL INFORMATION SERVICE
5285 PORT ROYAL ROAD
SPRINGFIELD, VIRGINIA 22161

FEDERAL GOVERNMENT AGENCIES AND THEIR CONTRACTORS REGISTERED WITH DEFENSE TECHNICAL INFORMATION CENTER SHOULD DIRECT REQUESTS FOR COPIES OF THIS REPORT TO:

DEFENSE TECHNICAL INFORMATION CENTER
CAMERON STATION
ALEXANDRIA, VIRGINIA 22314

CURITY CLASSIFICATION OF THIS PAGE

REPORT DOCUMENTATION PAGE

Form Approved OMB No. 0704-0188

a REPORT SECURITY CLASSIFICATION: UNCLASSIFIED

1b. RESTRICTIVE MARKINGS:

a SECURITY CLASSIFICATION AUTHORITY:

b. DECLASSIFICATION / DOWNGRADING SCHEDULE:

3. DISTRIBUTION / AVAILABILITY OF REPORT: Approved for public release. Distribution unlimited.

. PERFORMING ORGANIZATION REPORT NUMBER(S): Contract F08635-85-K-0052

5 MONITORING ORGANIZATION REPORT NUMBER(S): ESL-TR-89-73 Vol III

a. NAME OF PERFORMING ORGANIZATION: North Carolina State University

6b OFFICE SYMBOL (If applicable):

7a. NAME OF MONITORING ORGANIZATION: Air Force Engineering and Services Center

c. ADDRESS (City, State, and ZIP Code): Department of Mechanical & Aerospace Engineering, Raleigh NC 27695-7910

7b. ADDRESS (City, State, and ZIP Code): HQ AFESC/RDCS, Tyndall AFB FL 32403-6001

a. NAME OF FUNDING / SPONSORING ORGANIZATION:

8b. OFFICE SYMBOL (If applicable):

9. PROCUREMENT INSTRUMENT IDENTIFICATION NUMBER: Contract F08635-85-K-0052

c. ADDRESS (City, State, and ZIP Code):

10 SOURCE OF FUNDING NUMBERS

PROGRAM ELEMENT NO.	PROJECT NO.	TASK NO	WORK UNIT ACCESSION NO.
6.2	2673	0046	

1. TITLE (Include Security Classification)

Scaling Problems for Wave Propagation in Layered Systems Vol III

2. PERSONAL AUTHOR(S)

Sorrell,F.Y.;Horie,Y.;Whitfield,J.K.;Lee,S.H.;Park,J.K.

13a. TYPE OF REPORT	13b. TIME COVERED	14. DATE OF REPORT (Year, Month, Day)	15. PAGE COUNT
Final	FROM Mar85 TO Mar88	September 1989	262

16. SUPPLEMENTARY NOTATION

Availability of this report is specified on reverse of front cover

17. COSATI CODES		
FIELD	GROUP	SUB-GROUP

18. SUBJECT TERMS (Continue on reverse if necessary and identify by block number)

Gas gun; Scaling; Layered systems; Buried model structures; Ground-shock loading, Coventional, Wave propagation

19. ABSTRACT (Continue on reverse if necessary and identify by block number)

This Technical Report consists of three volumes. Volume I, Executive Summary, Introduction and Laboratory Test Program, describes the gas gun facility and technique and correct scaling for test models. Volume II, Wave-Analysis Program for the Response of Buried Model Structures, describes the computer code for wave propagation analysis of buried model structures under ground-shock loading. Volume III, Experimental and Numerical Program, covers methods of laboratory simulation of ground shock loading from a conventional weapon and develops a unified numerical simulation of ground-shock loading and structural response.

20. DISTRIBUTION / AVAILABILITY OF ABSTRACT: ☒ UNCLASSIFIED/UNLIMITED ☐ SAME AS RPT ☐ DTIC USERS

21. ABSTRACT SECURITY CLASSIFICATION: UNCLASSIFIED

22a. NAME OF RESPONSIBLE INDIVIDUAL: Diane B. Miller, Capt, USAF

22b. TELEPHONE (Include Area Code): (904)-283-3728

22c. OFFICE SYMBOL: HQ AFESC/RDCS

D Form 1473, JUN 86 Previous editions are obsolete. SECURITY CLASSIFICATION OF THIS PAGE

(The reverse of this page is blank.)

PREFACE

This report was prepared by North Carolina State University, Raleigh, NC 27695-7910, under contract number F08635-85-K-0052, for the Air Force Engineering and Services Center, Engineering and Services Laboratory, Airbase Structures and Weapons Effects Branch (AFESC/RDCS), Tyndall AFB, FL 32403-6001. Lt Col Robert J. Majka and Capt Diane B. Miller were the government technical program managers. This report summarizes work accomplished between 1 March 1985 and 1 March 1988.

This report has been reviewed by the Public Affairs office and is releasable to the National Technical Information Service (NTIS). At NTIS, it will be available to the general public, including foreign nations.

This technical report has been reviewed and is approved for publication.

Diane B. Miller
DIANE B. MILLER, Capt, USAF
Project Officer

Robert J. Majka
ROBERT J. MAJKA, Lt Col, USAF
Chief, Engineering Research Division

William S. Strickland
WILLIAM S. STRICKLAND
Chief, Airbase Structures and
Weapons Effects Branch

James R. VanOrman
JAMES R. VAN ORMAN
Deputy Director, Engineering and
Services Laboratory

(The reverse of this page is blank.)

TABLE OF CONTENTS

LIST OF FIGURES

LIST OF FIGURES
(CONCLUDED)

LIST OF TABLES

SECTION I

INTRODUCTION

This report covers experimental work and numerical simulations through a contract modification to contract FO 8635 K 0052, "Scaling Problems of Wave Propagation in Layered Systems." The purpose of the contract was to investigate methods of laboratory simulation of the ground shock loading from a conventional weapon, and to develop a unified numerical simulation of the ground shock loading and structural response. Results from the original investigations is given in References 1 and 2. As indicated in Reference 1, the laboratory method of choice was the light gas gun, and recovery tests were conducted to demonstrate the suitability of the light gas gun for laboratory simulation. Subsequent to the recovery tests, it was deemed desirable to have instrumented test data to further confirm the performance of the light gas gun as used for the simulation. Therefore, additional work was conducted on instrumented tests to measure the load versus time, or loading profile, on the model test structures. Section II of this report covers the evaluation of suitable instrumentation for use in laboratory simulations, and a summary of the data obtained.

In addition to the instrumented tests, additional numerical simulations were performed. The purpose of these simulations were:(1) to investigate predictive capabilities of the wave-analysis computer program, developed in the original contract, for calculating the response of buried model structures subjected to conventional munitions, and (2) to consider the development of preliminary, but quantitative relationships for design analysis and performance prediction. Results from the numerical simulation and an evaluation of its accuracy and utility are given in Section III of this report.

SECTION II

EXPERIMENTAL PROGRAM

A. BACKGROUND/TASKS

This section of the report covers the additional experimental work performed in the contract modification. After the recovery tests conducted under the original contract, it was deemed desirable to have instrumented test data to further confirm the performance of the light gas gun as used for the simulation. Therefore, additional work was conducted on instrumented tests to measure the load versus time, or loading profile, on the model test structures. This section of the report covers the evaluation of suitable instrumentation for use in laboratory simulations, and a summary of the data obtained.

Most of this work was thus spent in developing laboratory instrumentation to measure loading profiles on a model structure loaded by the light gas gun. Tasks in the contract modification were for evaluation of manganin, PVDF, and strain gages for use in laboratory simulation. Early work found that strain gages were not suited for the present instrument needs, and hence the evaluation was extended to carbon gages as well. The data obtained were used to meet two objectives. The first was to quantify the loading parameters in the light gas gun simulation. Data with sufficient precision were obtained that when put in suitable nondimensional form, the loading conditions could be compared with field tests. Second, all data from instrumented laboratory tests were combined into a data set on strong shock propagation through sandy soil. These data give the shock attenuation for a number of different soil thicknesses and shock strengths.

This report covers, in order, the experimental setup used to conduct the tests and evaluate different instrumentation; the results of the tests, including an evaluation of the different gages; and a summary of the results, giving the data base on shock propagation through soil and on the range of nondimensional loading parameters that can be achieved.

B. EXPERIMENTAL TEST SETUP

All tests were conducted in the shock impact laboratory at the Department of Mechanical and Aerospace Engineering at N.C. State University. This facility is described in detail in reference 1. The gas guns used to produce shock loading and the mount was used to hold the test model are the same as those described in this report; however, the gages were mounted in a different configuration designed to accommodate multiple gages, including a rather large PVDF gage. The configuration in which the gages were mounted is shown in Figure 1.

This configuration allows up to three gages to be mounted on the model. The large size of the PVDF gage does not permit it to be mounted directly at the center of the model, hence in most cases an additional gage was mounted off-center and symmetrically opposed to the PVDF gage. A PVDF gage was used for all tests. In shot M032, a manganin gage was mounted under the PVDF gage. In all of the other shots, either PVDF gages or carbon gages were mounted both on the model center and at the off-center location shown in Figure 1. The initial stress to the soil cover was calculated from the Hugoniot based upon the projectile speed and the type of projectile and coverplate materials. The accuracy of this method was confirmed in prior testing reported by ESL-TR-87-73.

All data except shot M032 were taken with an analog-to-digital (A/D) burst data acquisition system, which records up to four channels of data at a sample rate of 500K samples/sec on each channel. Up to 32k data points can be stored on each channel, which far exceeds the length of any shot. Digital data obtained in this manner were then stored on disk, and data reductions were performed by computer. Loading profiles for all shots with data obtained with this system are given in Appendix A.

GAGE CONFIGURATION

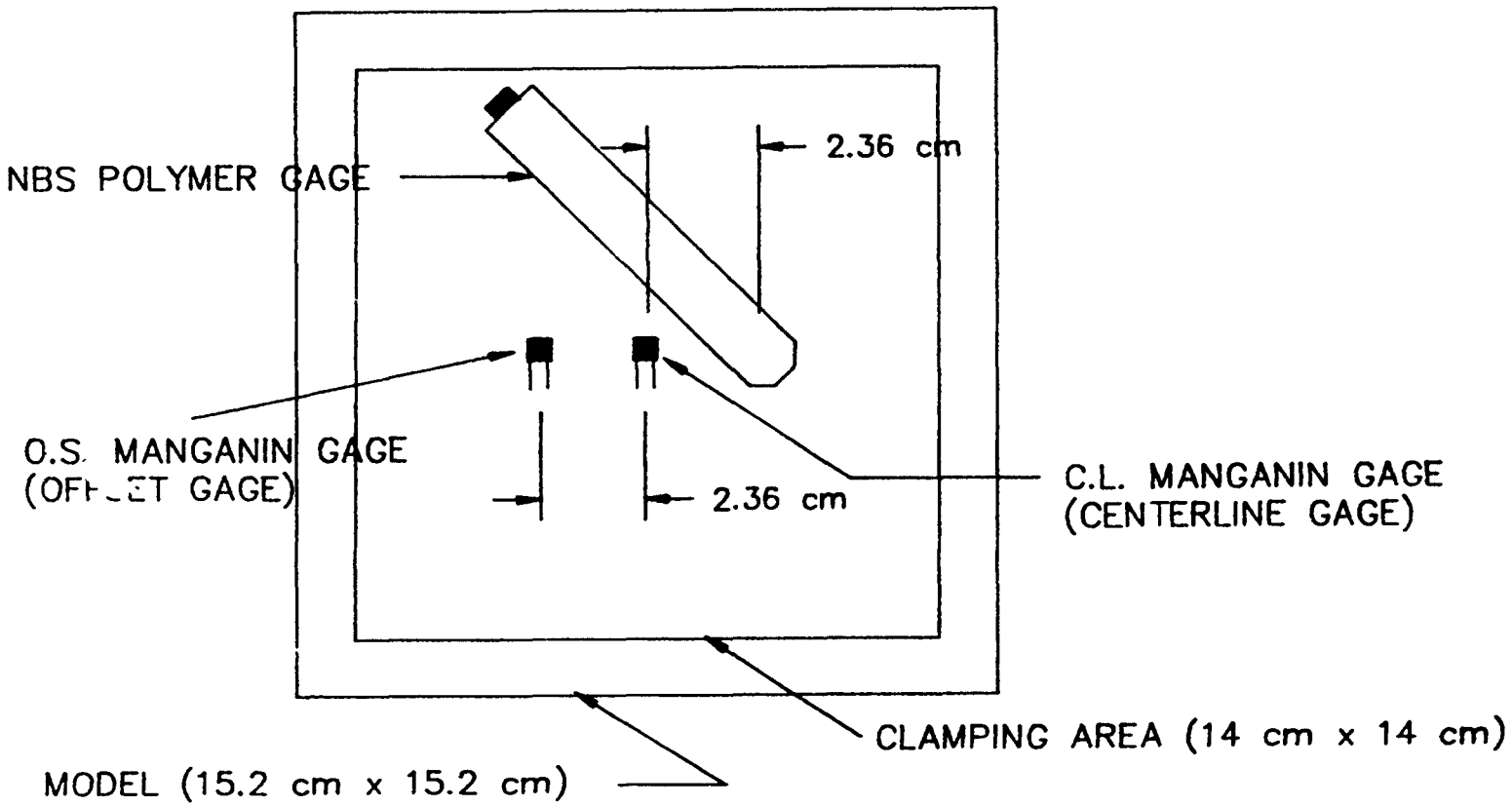

Figure 1. Diagram Showing Gage Locations.

C. TEST RESULTS

1. Data Summary

All tests conducted under the contract extension are summarized in Table 1. Test data given in this table include the shot number, the thickness of the soil cover, then peak input stress to the soil cover, and the resulting stress in the soil as the shock arrives at the model. These are the normal stresses in the soil at the front and at the back of the soil layer and are labeled as the input and output stress in the soil. Also included in Table 1, are the types of gages used in the test. With the exception of shot M032, all shots included one PVDF gage, mounted as shown in Figure 1, and an on-center and an off-center manganin or carbon gage. Strain gages were tried in several of the tests, but could not be used successfully. When the gages were mounted directly on the microconcrete model, the bond between the gage and the model failed. Strain gages mounted on a thin plastic sheet next to the model did not have sufficient sensitivity to give accurate data. In addition, there was some question as to the time response of this system. Therefore, after four unsuccessful attempts to use strain gages, they were abandoned and carbon gages were used in shot M041. The gages used in each shot are also given in Table 1.

Some preliminary data obtained prior to the contract extension were available from shots instrumented with manganin gages. These data were combined with the present data to form the data base used to establish shock attenuation through a soil layer. These data were then used to estimate the loading profiles that occurred in the recovery tests. Because these data were used in the analysis of the recovery tests and constitute a part of the overall data set used to establish shock attenuation, they are included in Table 1.

Although shot M032 employed both a PVDF and a manganin gage, the signal conditioning for the output of the PVDF gage failed. This shot had a relatively thick soil layer of 5 cm. The shock attenuation through the layer caused the normal stress at the Mangagin gage, located at the back of

TABLE 1. SUMMARY OF SHOTS AND TEST PARAMETERS

Shot No	Soil Thickness cm	Peak Stress -- MPa		Gaging		
		Input	Output	manganin	PDVF	Carbon
M032	5.0	136	8	X	X	
M035	2.5	144	16	X	X	
M036	3.2	137	14	X	X	
M037	3.2	137	18	X	X	
M040	8.6	220	12	X	X	
M041	7.8	227	14		X	X
Data From Prior Shots						
M027	2.3	198	52	X		
M030	3.2	134	25	X		
M031	1.14	156	74	X		
6-08	2.5	190	78	X		

the layer, to be at the lower limit of reliable manganin gage performance. Therefore, the peak stress was measured for this shot, but the loading profile was not deemed accurate and the loading profile is not included in the data set. Low sensitivity is the major problem with the manganin gages for shots with thick soil layers because the peak stress levels are often below 10 Mpa, which is lower than reliable operation of these gages. See Section III. Loading profiles for all of the other shots are included in Appendix A.

2. Gage Performance

Three of the tasks in the contract modification were to evaluate various types of gages for use in laboratory simulation of the ground shock loading on model structures. A summary evaluation of the gages used is given in this section. As previously mentioned, because strain gages were found unsuitable in the present application, carbon gages were also evaluated, in a search for suitable normal stress or pressure transducers, even though this evaluation was not in the tasks to be accomplished.

a. Strain Gages

Strain gages were tried in several of the tests, but could not be used successfully. When the gages were mounted directly on the microconcrete model, the bond between the gage and the model failed. Strain gages mounted on a thin plastic sheet next to the model did not have sufficient sensitivity to give accurate data. In addition the relation between strain in the plastic sheet and that in the microconcrete is not well defined. There was also some difficulty in maintaining the bond between the gage and the plastic sheet, although the bond held most of the time. Therefore, after four unsuccessful attempts to use strain gages, they were abandoned and carbon gages were used in shot M041. Because no data were obtained using strain gages, this gage is not included in the gage types listed in Table 1.

b. Manganin Gages

Manganin and carbon gages are piezoresistive sensors. They exhibit a change in resistance with normal stress. This change in resistance is normally measured by installation in one or more legs of a conventional Wheatstone bridge. However, sensitivity is a problem with all piezoresistive sensors, because the high bridge current needed for reliable measurements sensitivity may heat the gage.

Because manganin has proven useful to stresses greater than 100 GPa, it is the most widely used piezoresistive gage for measurements of shocks in solids (Reference 3). In the present application, however, the soil disperses the shock and the peak stress levels are much lower than in other solids. Because of this, the peak stress levels are usually at or close to the lower limit of reliable manganin gage response. Consequently the loading profile which contains even lower stresses is not measured reliably. An example of this is shot M032, in which stresses lower than reliable gage operation occurred. This is the reason that a alternative to the manganin gage is needed.

c. Polyvinylidene Fluoride (PVDF) Gages

PVDF is a piezoelectric sensor, which produces a charge propo·tional to normal stress. These sensors do not require a bridge and, hence current, through them to produce a signal; therefore, there is no heating of the gage. The sensitivity of these gages is ranges from 1KPa to 20 GPa, making them well suited for ground shock measurements in soil. Another advantage is that the gages are sturdy and hold up well when subjected to the large particle displacements that occur in soil. Because of their promise, a number of gages were made by the Polymers Division of the National Bureau of Standards (NBS) for test and evaluation. Four of these gages were used in the present evaluation.

The gages respond to normal stress on all surfaces, but with a different sensitivity. This means that the normal stress on the edges must also be known to interpret the output. Because of this the gages have been most successfully used in a uniaxial or hydrostatic state of stress. Under these conditions, they appear to be quite accurate. Measurements in a complex or unknown state of stress state are more difficult to interpret. To better define the gage performance under these conditions, Chung et al. (Reference 4) calibrated the gages in soil. This work indicates an increase in sensitivity of up to 2.5 times the sensitivity when calibrated hydrostatically. Soil has a low value of yield shear stress, and hence under strong shock conditions is expected to respond with approximately a

hydrostatic stress state. Consequently, the gage sensitivity in soil subjected to ground shock loading has not been completely defined. In the present experiments, the best correlation with either the manganin or carbon gages was obtained by using the hydrostatic calibration. Consequently, the correct gage sensitivity to use for shock testing in soil does not appear to have been entirely resolved.

As previously mentioned, four gages were available to use in the present evaluation. With this number of gages, multiple use or reuse of the gages was necessary to conduct enough tests for the evaluation. One gage was destroyed in the first shot it was used, and another gage was destroyed after two shots. These were mechanical failures of the base supporting the gage and were not related to the way the gage was constructed. The other two gages were used in two or more shots. A decrease in gage sensitivity was apparent after multiple use at these conditions (Table 1); although visual inspection showed no external damage, the gage sensitivity appeared to decrease. Because of this, it is recommended that PVDF gages be used only once in future tests, at least until this apparent decrease in sensitivity is better documented. The decrease in gage sensitivity combined with some question about the correct calibration procedure made accurate measurements difficult. Further work is needed before the PVDF gages can be used with confidence in an undefined and/or complex state of stress.

d. Carbon Gages

Carbon gages, like manganin gages, are piezoresistive. At lower shock stresses, carbon gages can be better suited because the resistance change is larger than that for manganin gages. Experimentally, the resistance change in carbon as a function of stress is reproducible up to 2 GPa (Reference 5). This is well within the range required for the present application. However, the resistance change in carbon with temperature is greater than manganin. This means that, because of gage heating, greater care is required to make accurate measurements.

One shot, M041, was made with both PVDF and carbon gages, arranged in the configuration shown in Figure 1. The gages did exhibit the expected change in resistance due to heating from the bridge current, however this was calculated and removed from the signal. This reduced gage output was consistent with prior tests and predictions. In addition, carbon is less brittle than manganin and therefore, holds up better when subjected to the relatively large particle displacements that occur in soil. At the present time carbon sensing elements appear to be one of the better techniques for our application Certainly, additional tests are to be desired before this can be confirmed.

3. Shock Propagation in Soil

The combined data in Table 1, consisting of test results from prior shots and from shots conducted through the contract modification, provide a data base on shock attenuation through soils of various thicknesses. Table 1 gives the peak stress as the shock enters the soil layer, labeled the input stress. After the shock traverse the soil layer, the peak stress was measured by one or more of the gages described above. The peak stress after propagation through the soil layer is labeled the peak output stress. The values given in Table 1 are the shock stress in the soil, not the shock stress as it is reflected off a boundary. The thickness of the soil layer is also given in Table 1. The shock attenuation is defined here as: peak output stress/peak input stress.

The shock attenuation verses soil thickness is plotted in Figure 2. The data consist of all shots in Table 1, and the individual data points are labeled by shot number. A least-squares curve fit to the data is shown as the solid line. The equation chosen for the curve fit was:

$$P_{out}/P_{in} = (t/t_o)^{\eta} \qquad (1)$$

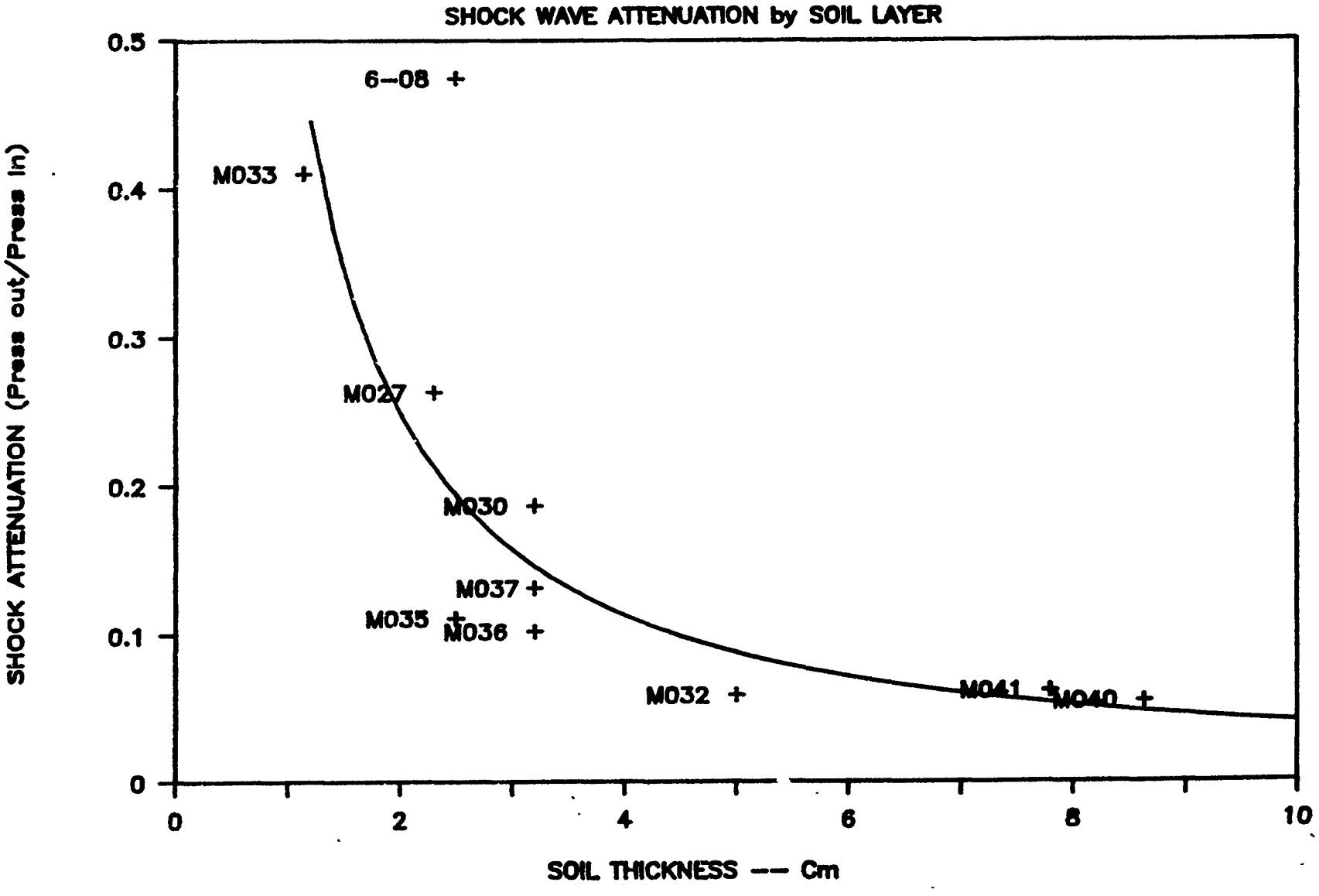

Figure 2. Shock Wave Attenuation in Soil Layer.

Where P_{out} = the peak output normal stress, P_{in} = the peak input normal stress, t_o is a reference thickness, and t = the soil thickness in cm. The least-squares curve fit to the data gave the value for t_o = 0.6 cm and the value for n = -1.136. This curve fit has an RMS error between the measured and calculated (from Equation (1)) shock attenuation of 0.104. If the data point associated with shot 6-08 is left out, the RMS error = 0.04. One consequence of this good agreement is that the shock attenuation depends primarily on only the soil thickness. Although there is not a wide range of peak input stress, there is no apparent dependence of shock attenuation on the peak stress levels. Shot 6-08 was with a much higher impulse, and is one of the data points that does not fit the curve well. Because this is a single data point, it is not possible to draw any well-founded conclusion; however, the observation is made.

The observation that the shock attenuation depends primarily on only the soil thickness means that the shock strength (peak shock output stress) after propagation through the soil layer can be estimated with good accuracy if the peak input stress and the soil thickness are known. As previously mentioned, the peak input stress can be accurately calculated from the projectile speed and the material of the coverplate and the projectile. The projectile speed was measured and the material of the projectile and coverplate as well as the soil thickness was known for all of the recovery tests. Therefore, the peak shock loading for all of the recovery tests can be calculated. This is the major objective of developing this data base.

The data presented in Figure 2 should be useful for predicting shock attenuation in dry soils. The data can be used for evaluation of numerical codes, or in estimating the shock attenuation in soils of various thicknesses. Because part of the shock attenuation in the present experiments is due to release waves from the edge of the soil layer, the results in Figure 2 can not be applied directly to shock attenuation in unbounded soil.

4. Nondimensional Loading Parameters

The major objective of the contract was to investigate the suitability of the light gas gun for laboratory simulation of the ground shock loading from conventional weapons on hardened structures. A number of recovery experiments were conducted to qualitatively compare failure modes in the laboratory simulation to those observed in field tests. These recovery experiments and the failure modes were described in the final report ESL TR 87-73. The data base given in Figure 2 can be used to quantify the results observed in the recovery tests. This is accomplished by using the data base in Figure 2 to estimate the peak shock loading on the model structures protected with a soil layer. The total impulse of the projectile is used to give the impulse on the model, thus, both the peak stress and the impulse that produced failure of the model structure can be estimated. If the peak stress and impulse are the major parameters that establish the failure criteria for a particular structure, marginal failure (when the structure just begins to fail) should depend primarily on these two parameters.

Therefore, failure of any specific structural design can be correlated with these two parameters. Note, however, that the combination of impulse and peak stress that produces failure will vary with size or design of the structure. Clearly, a more massive structure will require a larger impulse for failure. The objective of the present work requires a comparison of failure conditions (impulse and peak stress) of a laboratory scale experiments with field tests. This comparison requires that the failure criteria must be put in nondimensional form. ESL TR 87-73 discusses the proper scaling for laboratory experiments and includes proposed nondimensionalization of the impulse and peak stress appropriate for the present scaling conditions. Of the scaling parameters, the nondimensional impulse and peak stress are repeated here.

The nondimensional peak stress = P^* is:

$$P^* = \frac{P_{max}}{\sigma_y} \tag{2}$$

where P_{max} = the peak stress of the shock loading, and σ_y = the compressive yield stress of the concrete structure. The nondimensional impulse = I^* is given by:

$$I^* = \frac{I}{\sigma_y L^2 (\rho/E)^{1/2} L'} \tag{3}$$

where I = the total impulse of the loading (integral of normal stress over time), L = the length scale of the structure, ρ = the structural density, and E = the structural modulus of elasticity. Physically, the nondimensional impulse in Equation (3) is obtained by dividing by the product of force times time. $\sigma_y(L^2)$ has the dimension of force and $(\rho/E)^{1/2} L'$ has the dimension of time. For a rectangular plate this time is proportional to the natural frequency if L′ is the length of one side of the plate and proportional to time for an elastic wave to propagate through the plate if L′ is the plate thickness. For a fixed geometric configuration, the relation between the wall or plate edge length and the wall thickness is fixed, thus either dimension can be used. In the present nondimensionalization the edge length is used.

The calculated conditions of nondimensional impulse and peak stress that produced marginal failure in the recovery tests are plotted in Figure 3. Each point in the figure represents failure conditions for the same test model structure. However, structures with and without reinforcing bars are included in this figure. All of the data points shown were complete failures, except shot M024 which exhibited some cracking on the back surface but did not fail. A summary of failure mode at each data point follows:

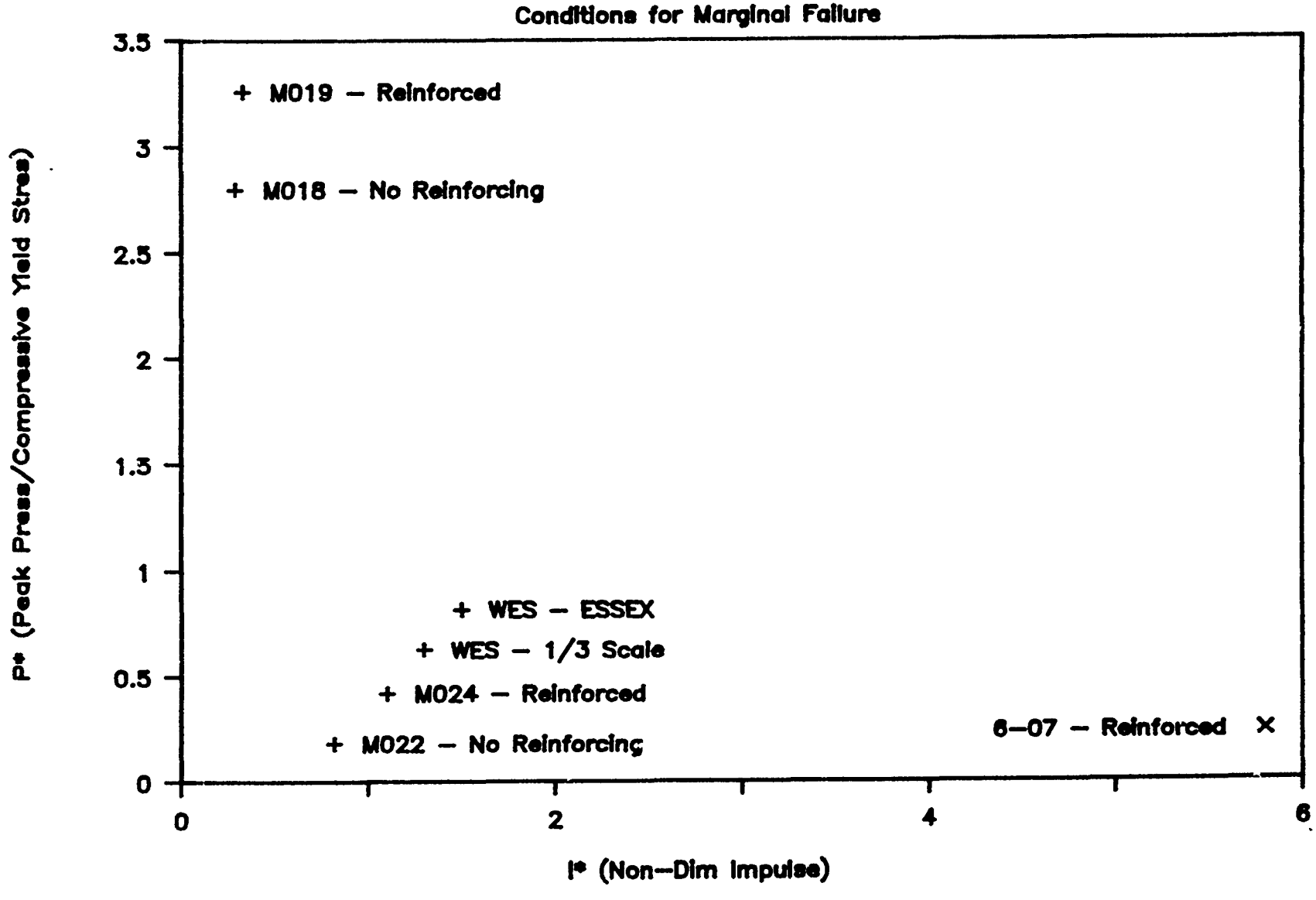

Figure 3. Plot of Nondimensional Loading Conditions That Produce Marginal Structural Failure.

Shot	Failure Mode
M018	Breech -- Spall
M019	Breech -- Spall
M022	Breech -- Bending
M024	Cracking on Tensile (back) Surface
6-07	Breech - Bending/Flexure

It is evident that the failures at high peak stress and relatively low impulse were spall type failures, whereas the failures at lower peak stress and larger impulse were bending failures. The test model in this case was a scale model of a thick wall (length to thickness ratio = 4) structure tested at Waterways Experiment Station (WES). (References 6 and 7) Because the failure criteria or the parameters that produced failure are in non-dimensional form, the data from the WES tests can be plotted on the same figure. The failure conditions for the test model and those from the WES experiments are consistent, indicating the validity of the scaling as well as the test procedure.

The failure mode for all of the test models was either by spall, or by bending. In most cases, the wall of a hardened structure is breached by the so-called punch failure, where a section of the wall is "punched out" by local shearing. The reason the test models did show punch failure is probably because the loading was not at the intermediate range of peak stress and impulse observed in the WES tests. In addition, the thick wall structure may make the shear type failure less likely. The failure mode of the WES-ESSEX test is by shear, following earlier minor deterioration in bending, and the response in the WES - 1/3 Scale test is described as flexure/membrane.

SECTION III

NUMERICAL SIMULATION

A. BACKGROUND/TASKS

This section of the report covers work in numerical simulation that was conducted on the contract modification. As previously stated, the objectives were: (1) to investigate predictive capabilities of the wave-analysis computer program, developed in the original contract, for calculating the response of buried model structures subjected to conventional munitions, and (2) to consider the development of preliminary, but quantitative, relationships for design analysis and performance prediction.

The computer program is a two-dimensional, plane strain, Lagrangian finite-difference program using artificial viscosity to smooth shock fronts. A detailed description of the program is given in Reference 2, the final report on the contract. The program contains constitutive models for investigating the response of buried structures to ground-shock loading from beginning to end in a unified fashion. They are: (1) a standard hydrodynamic-elastic-plastic model for solids such as concrete, (2) a model specially developed for soils, and (3) an explosive model based upon Chapman-Jouget detonation theory. The standard solid model has a tension cutoff scheme to handle fracture on the basis of maximum tensile stress. The soil model was developed to deal with the influence of porosity on the inelastic behavior of materials in a physically consistent manner so that phenomena such as shear enhanced pore compaction can be represented.

Previous model calculations presented in the final report focused on laboratory concrete frames in which ground shock was simulated by use of a light gas gun. The calculations showed: (1) that predicted features were consistent with experimental observations regarding modes of failure, load profiles at concrete surfaces, and their interrelationships, and (2) that numerical simulation could provide a basis for interpreting the response

behavior of buried structures subjected to high pressure ground shock loading by directly focusing on shock waves that excite the structures.

The purpose of this work was to further demonstrate the applicability of the program for calculating the response of buried structures subjected to localized chemical explosions. Most of the work was to simulate the ground-shock loading of a buried structure in a unified fashion including explosive detonation, ground-shock propagation, and soil-structure interactions. Also, an attempt was made to establish a peak-pressure impulse relationship to predict failure mechanisms through parametric numerical calculations.

B. CONFIGURATION FOR MODEL ANALYSIS

The analysis configuration, shown in Figure 4, is one of the experimental configurations used in recent test series run by the Engineering and Services Laboratory, Tyndall AFB (see Reference 7). It represents a one-third scale model of a typical command and control center structure. The primary goal of these tests was to determine the response of a shallow-buried concrete structure subjected to the effects of localized loading from the detonation of conventional weapons near the structures. The data were made available to us by Mr. John R. Hayes of Tyndall AFB, one of our technical monitors on the project. It was the only instrumented test for which we had information on critical parameters such as pressure histories at the interface between soil and concrete slab and modes of failure.

Unfortunately, however, few data were available to determine constitutive properties of the materials used in these tests. Therefore, inert properties such as the compressive strength of soil under high pressures were assumed to be the same as those used for the previous calculations described in the final report. The explosive source was assumed to be a TNT sphere without a case. Since the code is two-dimensional, the surface area of the sphere was scaled on the basis of an

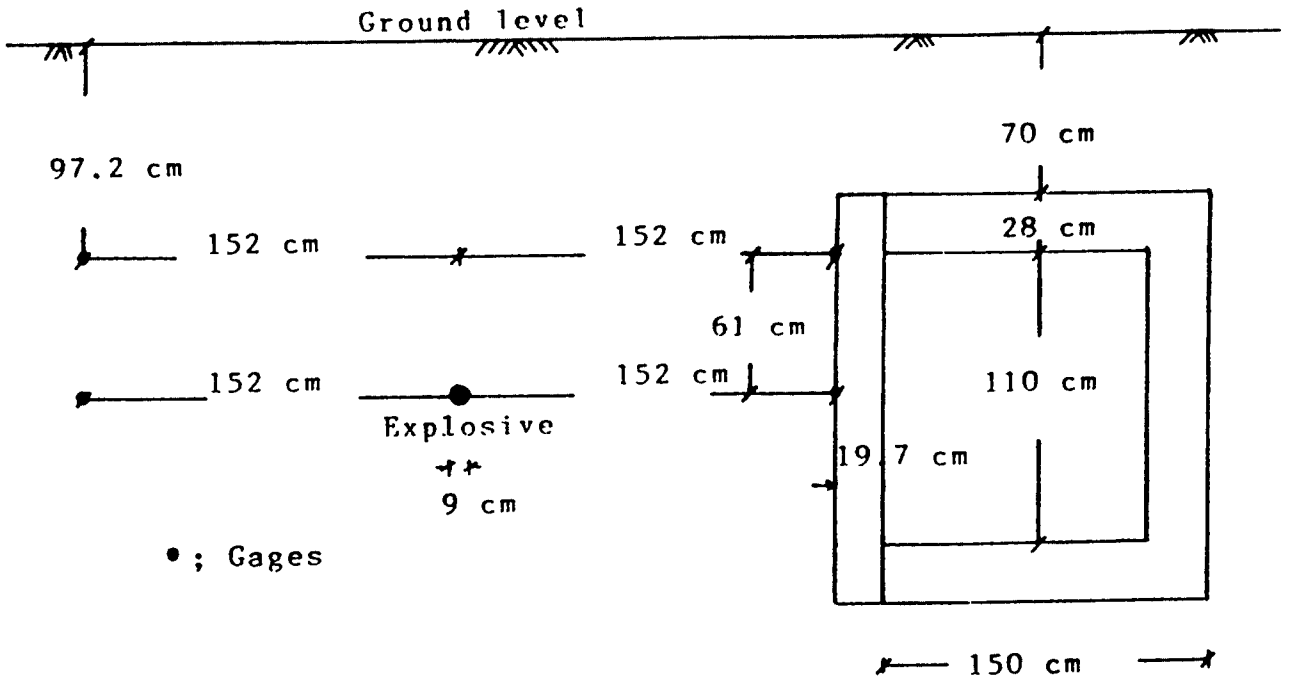

Figure 4. Configuration of Air Force Experiment (Test 7).

MK-83, 454 kg(1,000-pound) bomb. The calculated Chapman-Jouget pressure was approximately 260 kb (3 by 10 6 psi).

In numerical simulation, the response of the buried structure subjected to the effects of the TNT explosion was investigated in terms of standoff distance. However, because of a fundamental difference between the scaled experiment, a three-dimensional test, and the simulation, a plane-strain calculation, a direct comparison of the two is not possible. The calculations were intended for investigating the qualitative features of model behaviors.

The remainder of this section is divided into two subsections: subsection C describes selected output of the model calculations including free field calculations and subsection D discusses this output.

C. MODEL OUTPUT

This section presents results from calculation of two test configurations, corresponding to short and long standoff distances as well as those corresponding to a free-field calculation. The long standoff distance corresponds to that of the Air Force test configuration shown in Figure 4. The purpose of the free-field calculation was to investigate the nature of ground shock threat from close-in detonation. The determination of an equivalent load from free-field ground shock at a prescribed standoff distance is the first step in traditional procedures for the design of protective structures against impulsive loadings.

1. Free-Field Solution

Figures 5 and 6 show features of free-field ground shock propagation in terms of stress and particle-velocity histories. However, the values of peak stress observed in the field tests were much smaller than the calculated values. The primary cause of this discrepancy was attributed to material properties and the difference in the number of spacial dimensions: two vs. three. In plane strain the values of peak stress and peak particle

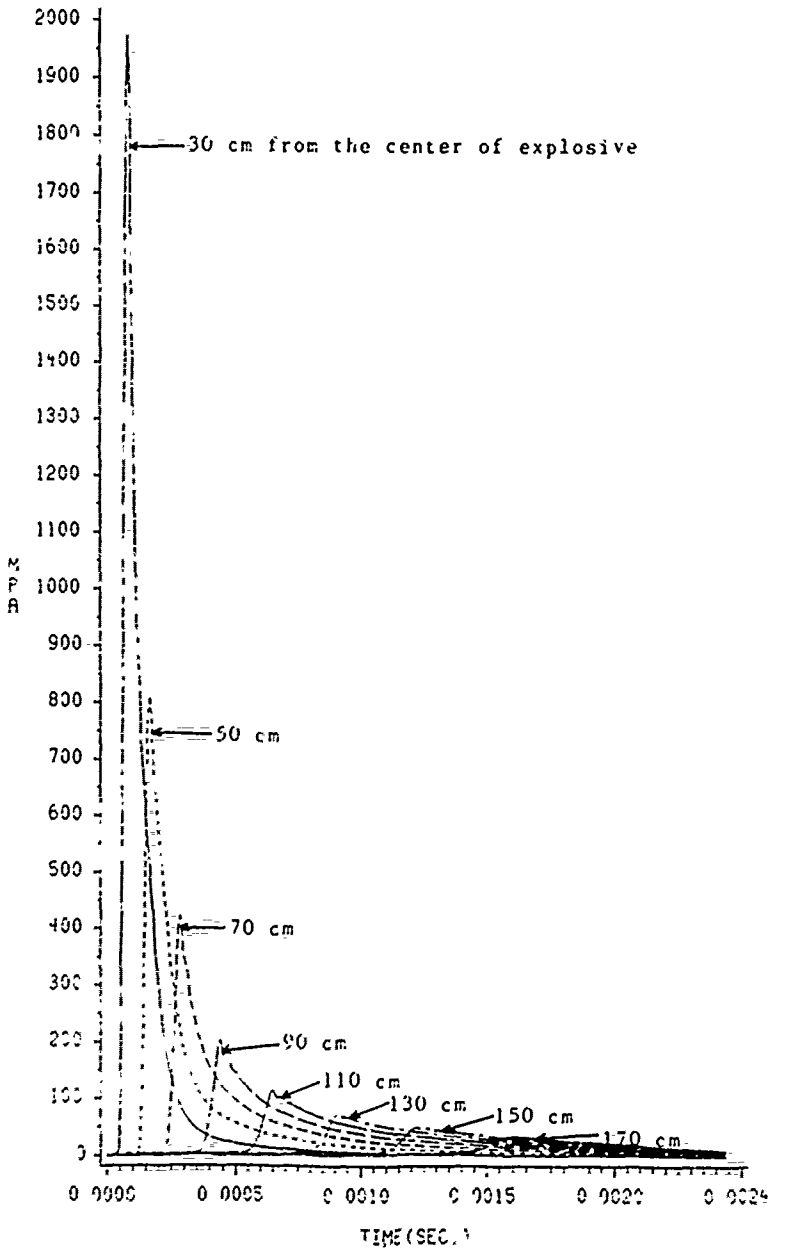

Figure 5. Calculated Stress Histories at Various Distances from Explosive Center.

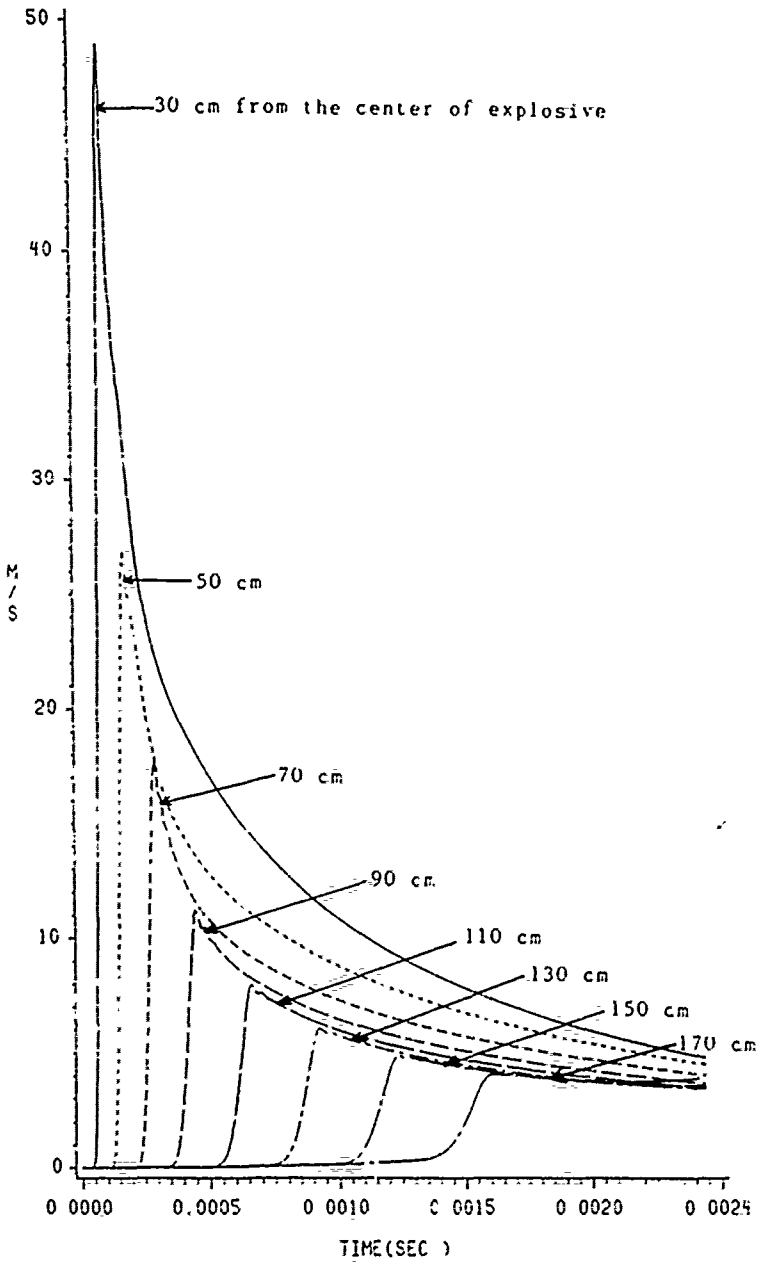

Figure 6. Calculated Particle Velocity at Various Distances from Explosive Center.

velocity were scaled on the basis of the square root of the cross sectional area of the explosive charge. Therefore, no attempt was made to adjust the magnitude artificially.

Figures 7 and 8 show the time of arrival of shock front and its rise time. These time scales are often used in traditional approach (e.g. Reference 8) to predict ground shock threat on the basis of empirical formulas. These figures show that the traditional assumption of constant wave speed defined as distance dived by the time of arrival and the proportionality of the rise time to the arrival time is not applicable for close-in detonation. The calculation is a demonstration of evidence (Reference 9) that conventioanl data base and idealizations are insufficient for bombs detonating very close to their targets. The increase of the rise time at large distance is a numerical artifice caused by finite-size calculations. It was created by wave reflections from boundaries.

2. 70-cm Standoff Calculation

This configuration is a model system and represents a very close detonation. the purpose of this model calculation was to illustrate the effects of ground shock curvature as it interacts with the structure.

Figures 9-11 show normal stress contours (horizontal component) at 265-, 378- and 434-microsecond-integrals from the time of detonation. Two noteworthy features are shown in these diagrams. The first is the propagation of a localized high pressure region along the concrete wall nearest to the explosive extending from center to "upper" support of the wall. This is a curvature effect of ground shock from a close-in detonation. The second is the development of large tension in a central region of the wall (Figure 11). This well-known phenomenon results from the reflection of a triangular compression wave from inner free surface of the concrete slab. This eventually leads to localized spalling or breaching of the slab.

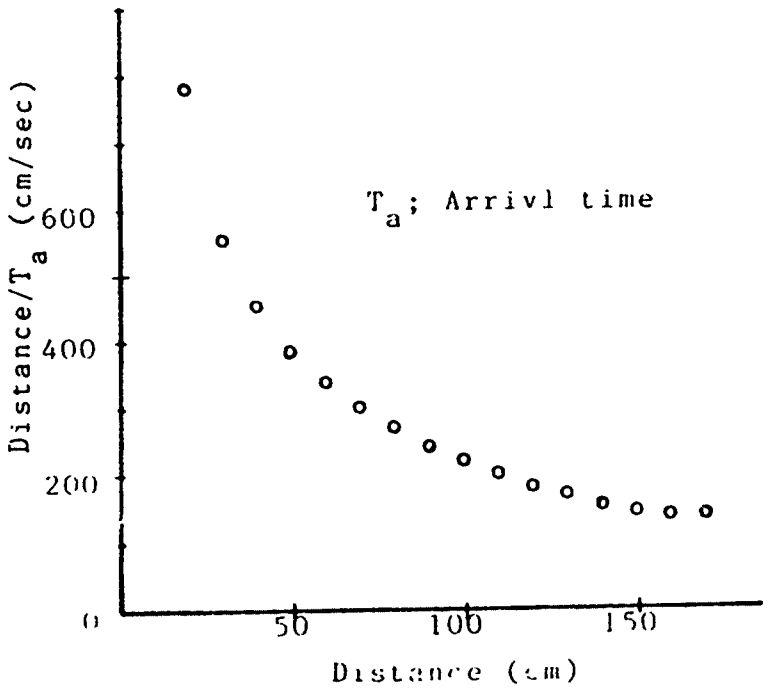

Figure 7. Calculated Wave Speed Based Upon Distance/Arrival Time.

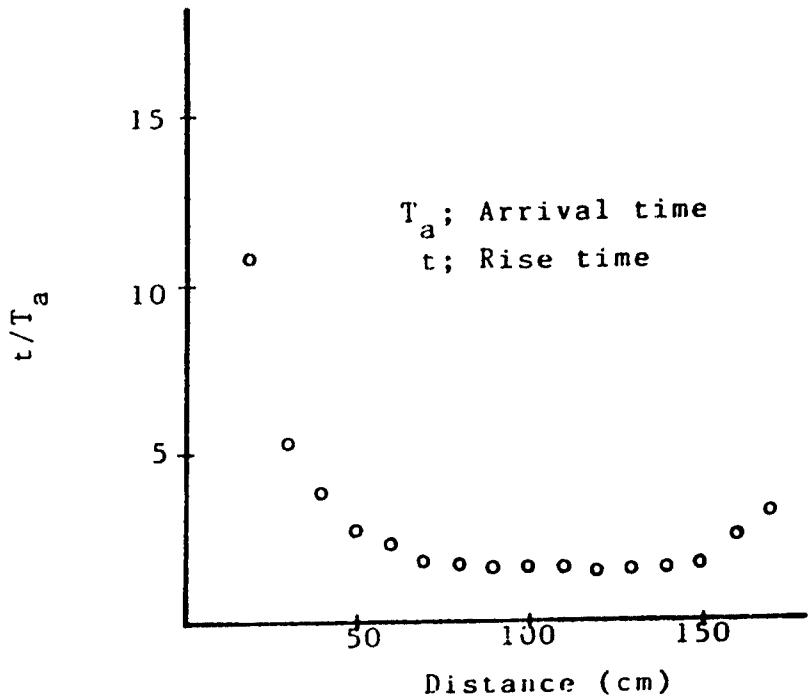

Figure 8. Calculated Ratio of Arrival Time to Rise Time.

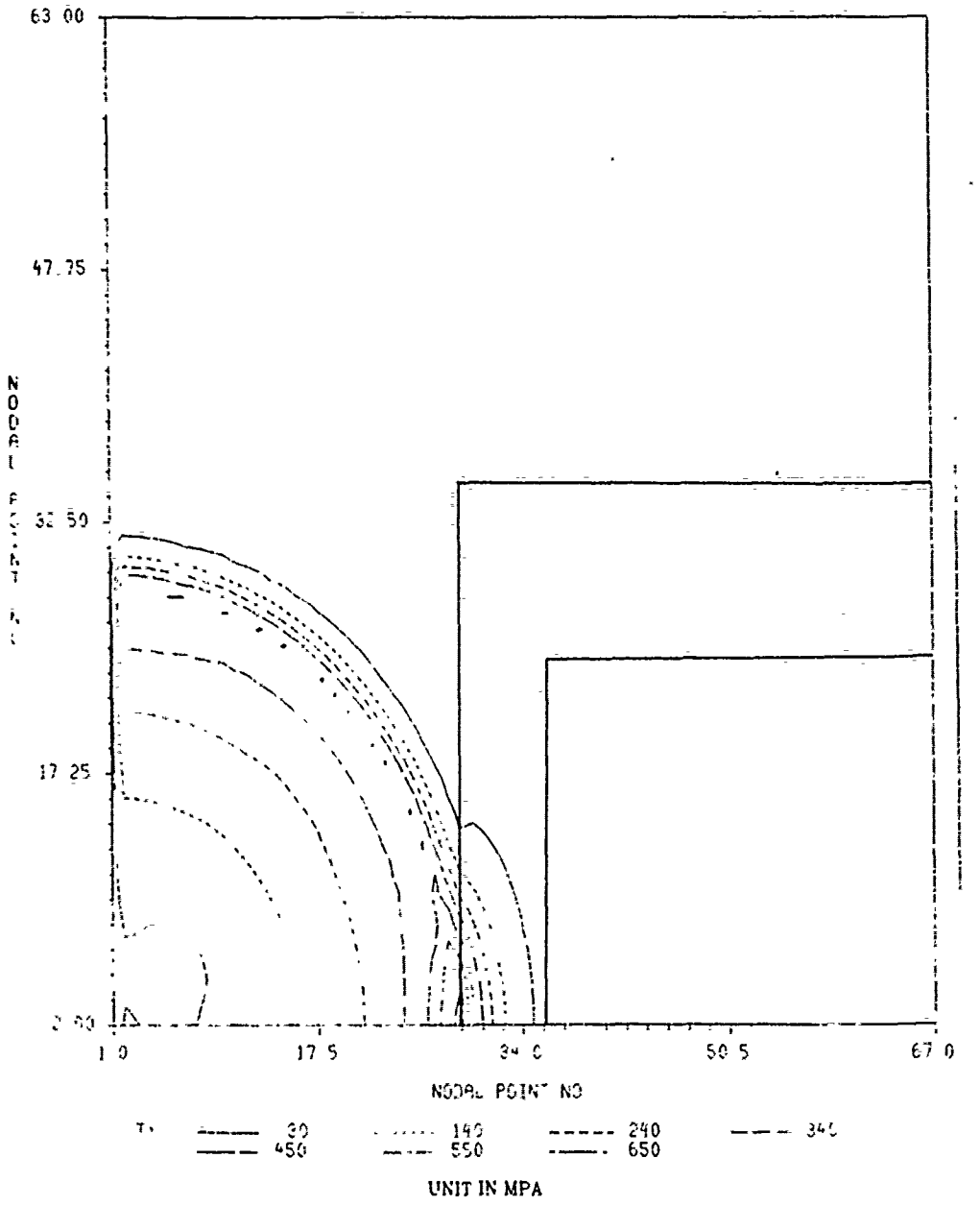

Figure 9. Horizontal Normal Stress Contours from 70 cm Standoff Calculation at 265 Microseconds.

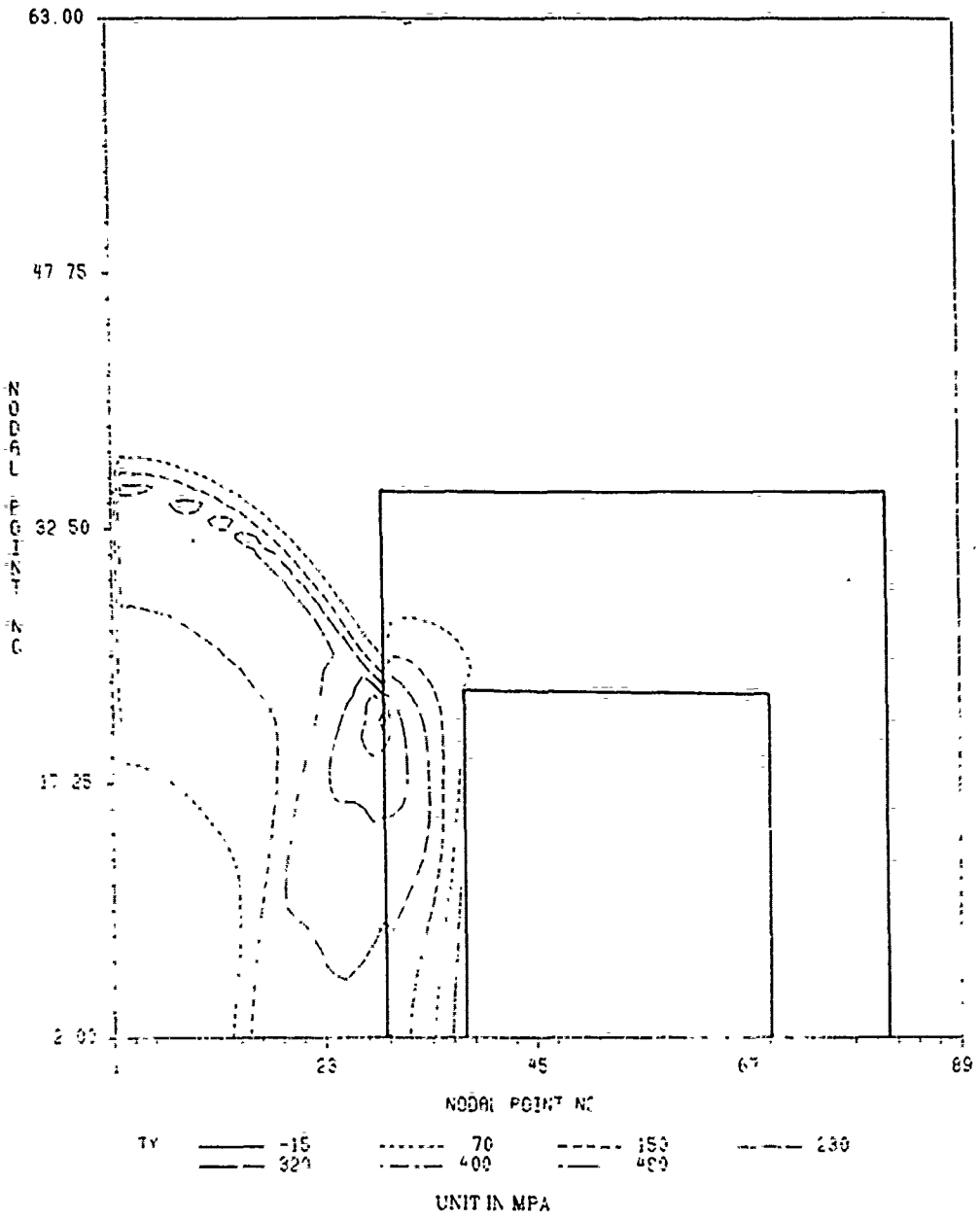

Figure 10. Horizontal Normal Stress Contours from 70 cm Standoff Calculation at 378 Microseconds.

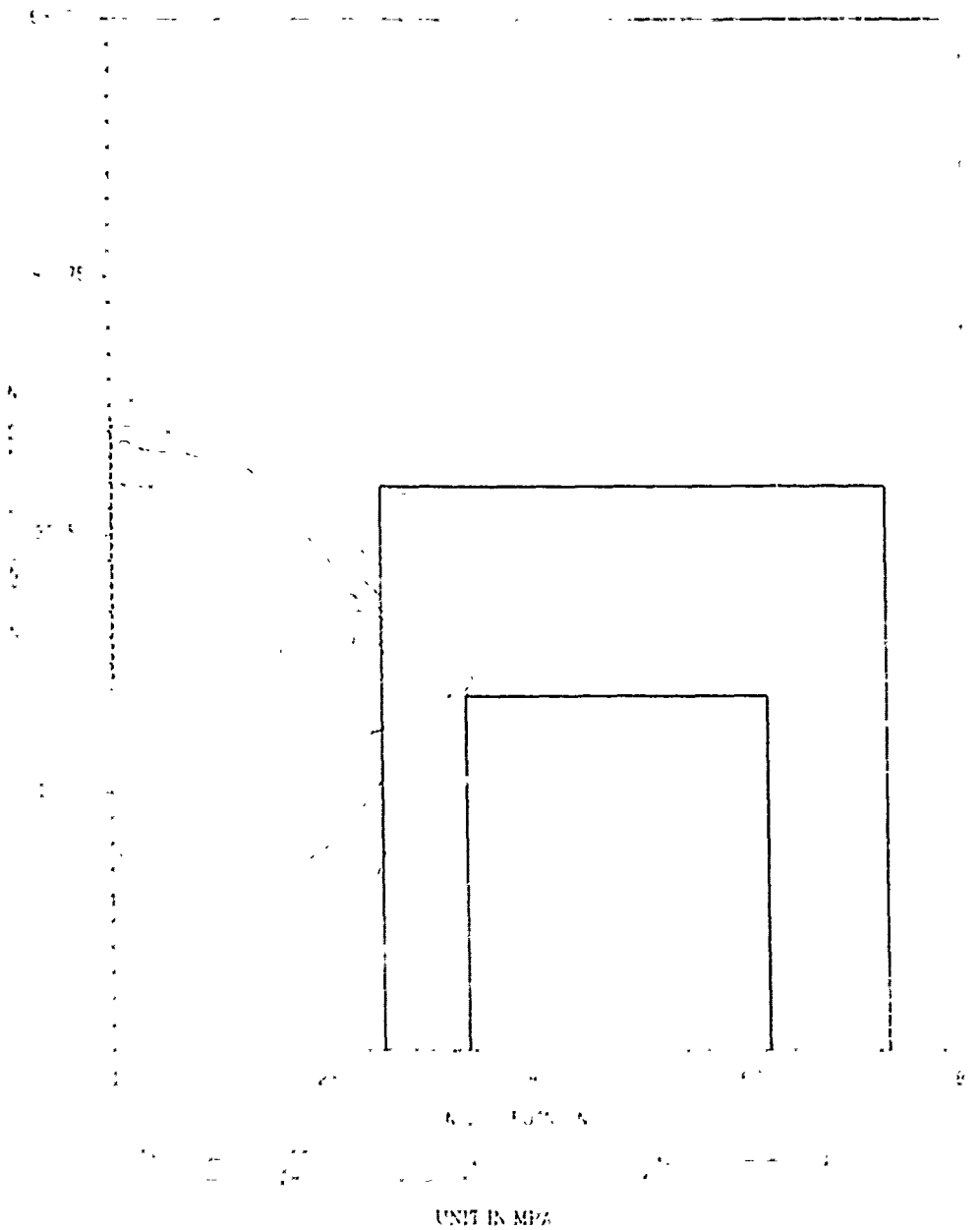

Figure 11. Horizontal Normal Stress Contours from 70 cm Standoff Calculation at 434 Microseconds.

3. 150 cm Standoff Calculation

This configuration represents Test 7 of the Air Force experiment. The calculation of longer standoff distances was not possible because of the longer computing times required.

Stress contours similar to those in Figures 9-11 are shown in Figures 12-14. These figures show the disappearance of both the propagating high pressure region and the spall tension. This disappearance was caused by the changes in the properties of ground shock generated at the 150-cm standoff distance. These changes are: (1) that the wave front of the shock, as it arrives at the face of the closest wall, becomes almost parallel to the surface, and (2) that the shock is so dispersed that the load is almost quasistatic (Figure 6). Therefore, if there is any failure of the wall slab, it is definitely of bending type. The pattern of stress contours in Figures 13 and 14 is associated with a flexural deflection of a fixed beam. The transition of failure mode from a spall type to a flexure type will be considered again in the next section.

Figures 15 and 16 show a comparison of interface pressure and impulse with those of the free-field solution at center and "upper" support of the wall, respectively. As is discussed earlier, it is not possible to compare directly these results with those measured in the actual field tests. The magnitude of ground shock was too large. However, the qualitative features of the calculated results are in agreement with experimental observations (Reference 7). Notable examples are: (1) a crossing of the impulse curves in Figure 16 and (2) a faster decay of interface pressure than that of free-field presure.

4. Impulse-Pressure Relationship

As demonstrated in Section I of this addendum, peak stress-impulse can be used as indicators of the critical load for impulsively loaded structures such as the one under investigation.

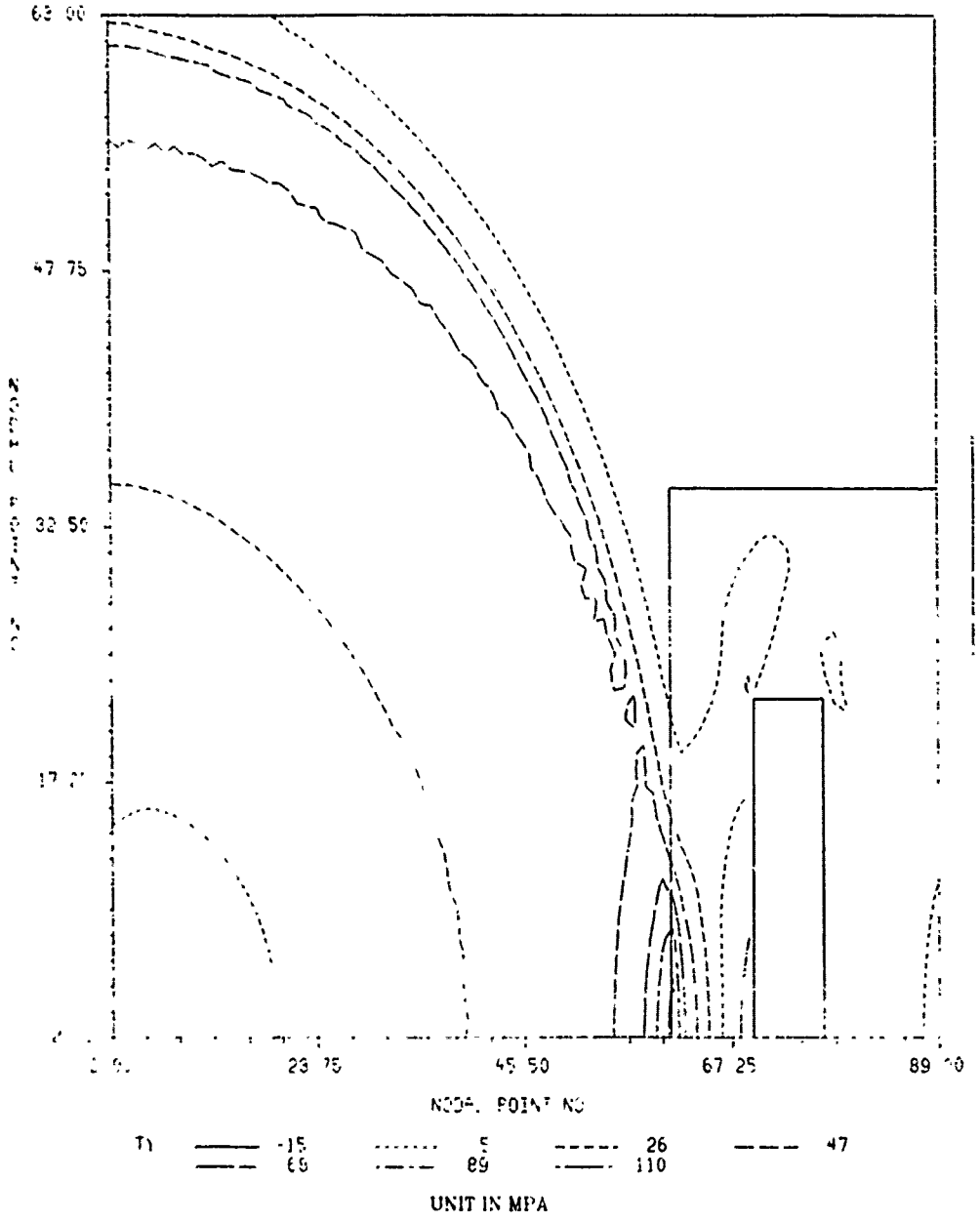

Figure 12. Horizontal Normal Stress Contours from 150 cm Standoff Calculation at 1.15 Milliseconds.

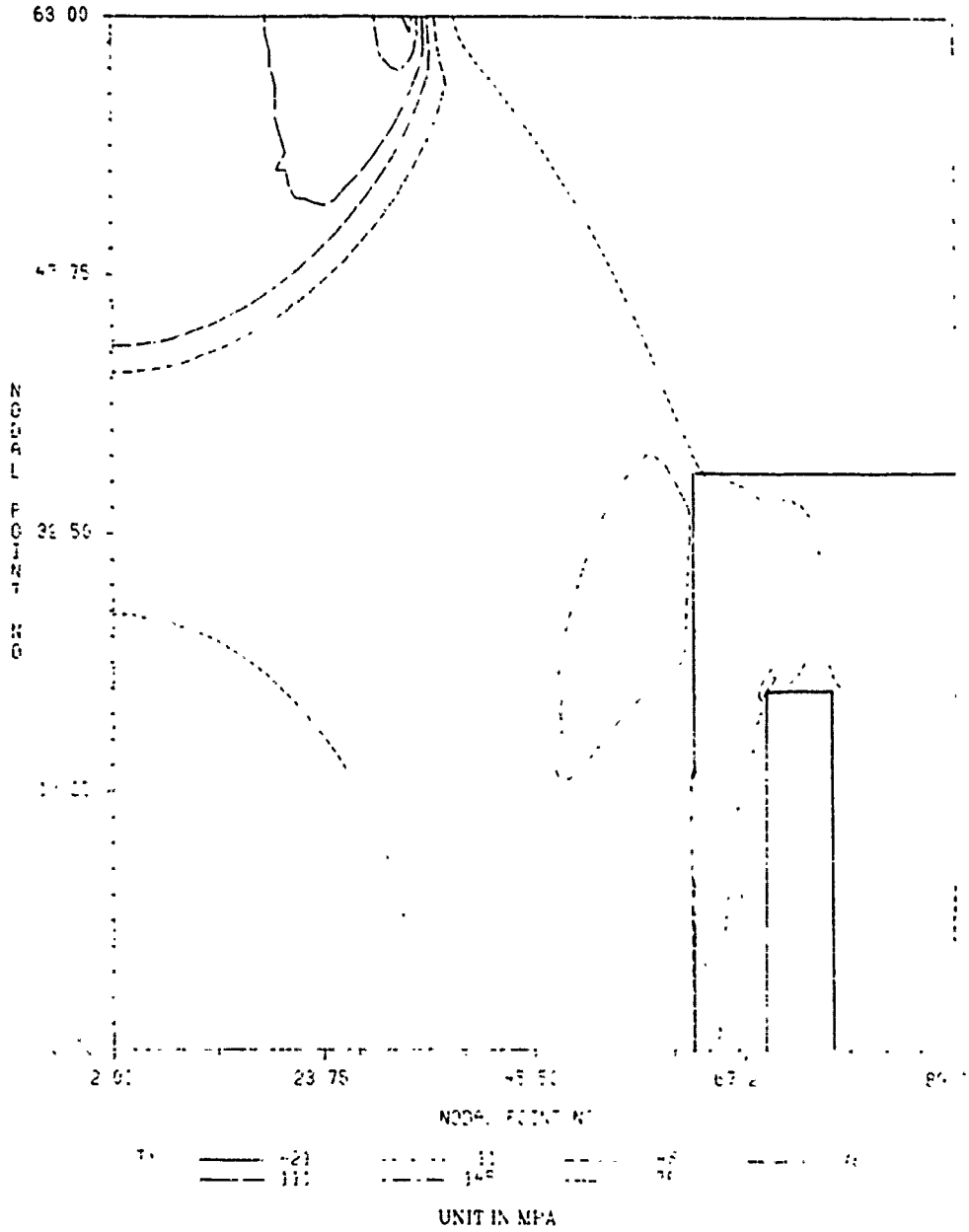

Figure 13. Horizontal Normal Stress Contours from 150 cm Standoff Calculation at 1.49 Milliseconds.

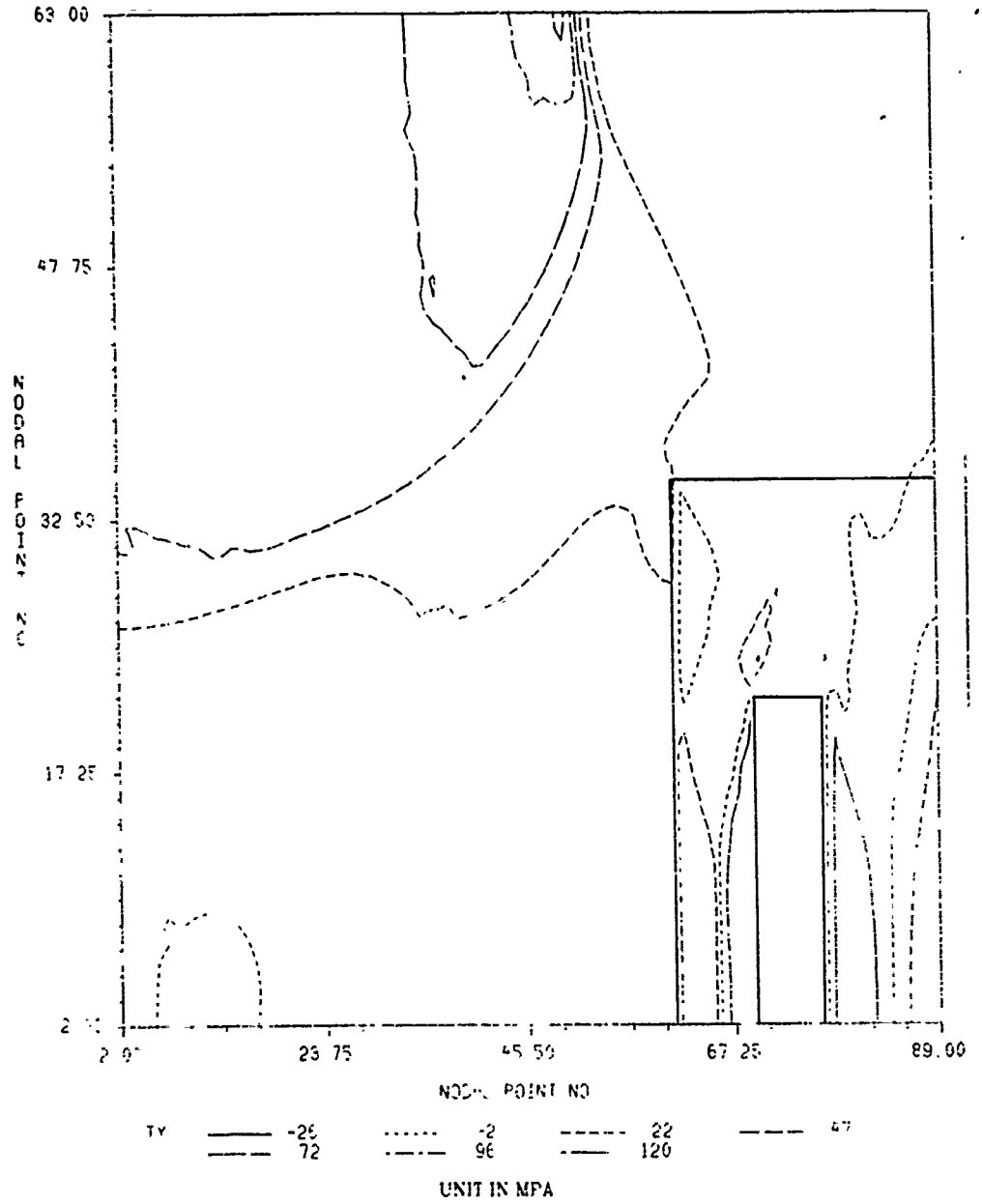

Figure 14. Horizontal Normal Stress Contours from 150 cm Standoff Calculation at 1.83 Milliseconds.

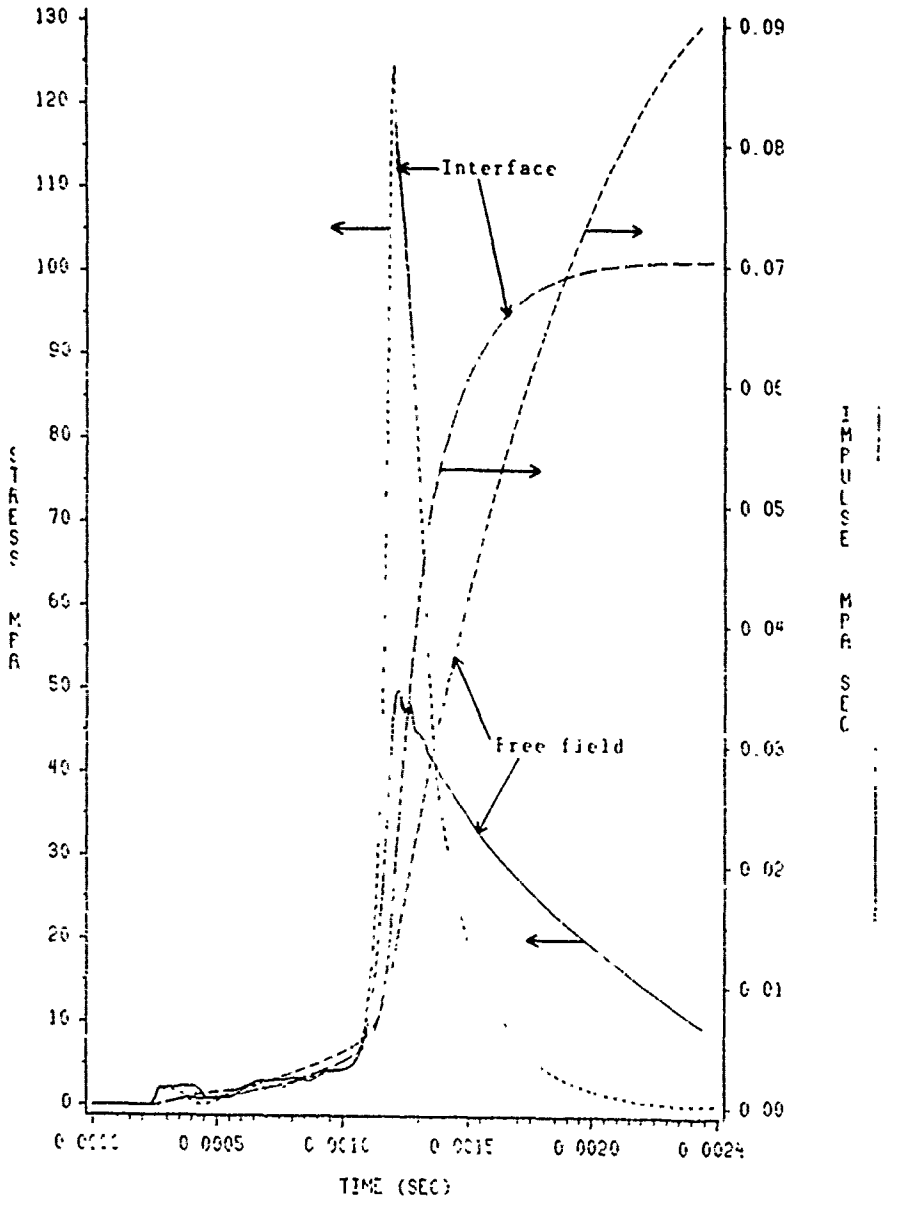

Figure 15. Comparison of Pressure and Impulse Histories at Center of Concrete Slab between Free-Field and 150 cm Standoff Distance Calculations.

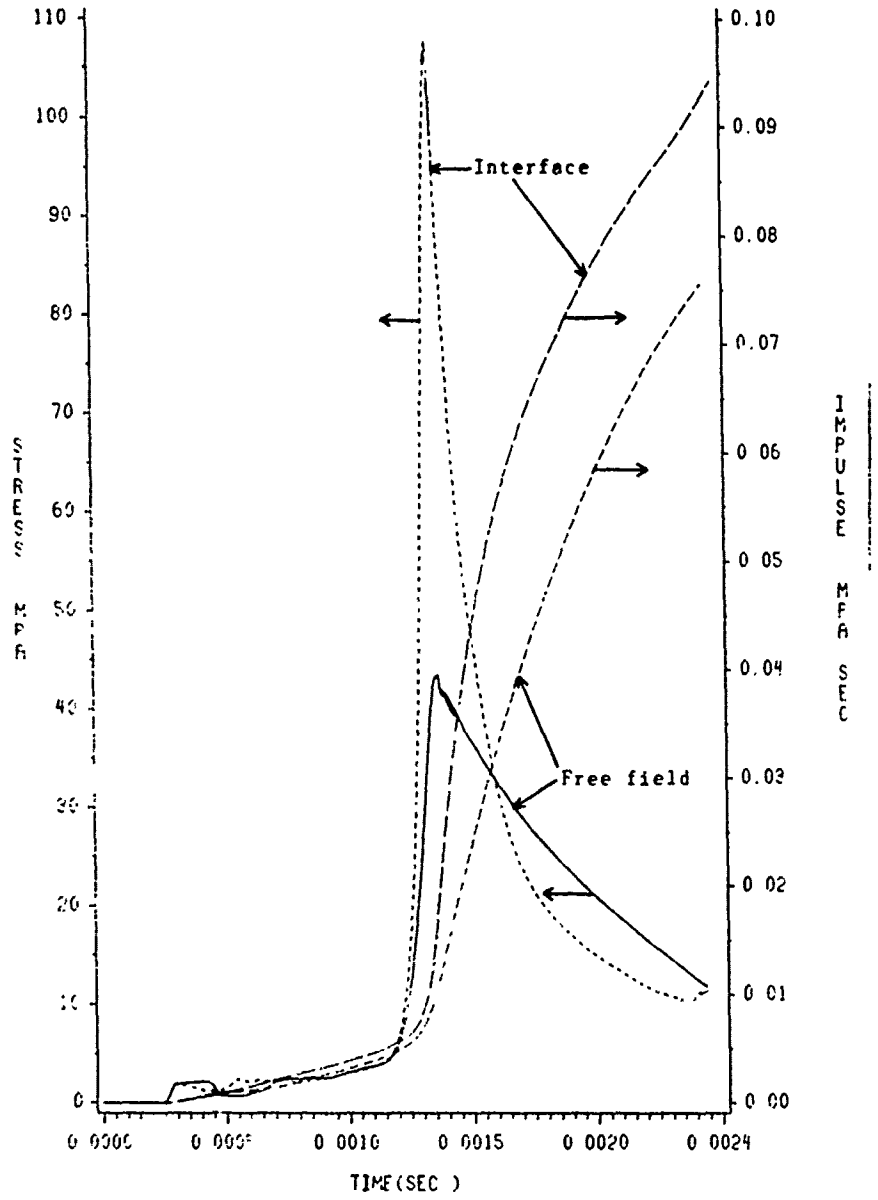

Figure 16. Comparison of Pressure and Impulse Histories at Support of Concrete Slab Between Free-Field and 150 cm Standoff Distance Calculations.

However, critical loads generated by such an analysis depend on an assumed mode of failure, typically of flexural type (Reference 10). Localized failure such as spalling cannot be included in such an analysis, because it depends upon complex wave-structure interactions.

Therefore, a numerical parametric study was conducted to examine the peak stress-impulse relationship as it relates to failure modes. Results were summarized in Figure 17. It shows a comparison of peak stress and impulse between free-field calculations and calculations with the structure for three standoff distances. Two observations can be made. The first is that the crossing of peak stress-impulse curves for the structure occurs in the same region as that indicated by stress contours. That is, the transition from spalling to bending failure takes place at the standoff distance of about 110 cm. The second is that although the peak stress increases as the ground shock reflects from concrete slab, the impulse decreases. The latter may be attributed to factors such as increased consolidation of soil, the effect of free surface, etc. This phenomenon may be another evidence that a layered system offers better protection than a comparable monolithic system.

D. CONCLUSIONS

The results described above indicate that this wave analysis program can deal with the interaction of nonnuclear munitions with buried structures in a unified fashion. Since traditional idealizations and data bases seem insufficient for loading from the detonations of conventional weapons near the structures, numerical simulation combined with model testing may prove to be cost-effective in generating a data base for analysis and aid in the design of buried structures. The principal limitations are the generality of a given program and the uncertainty in the description of material behaviors.

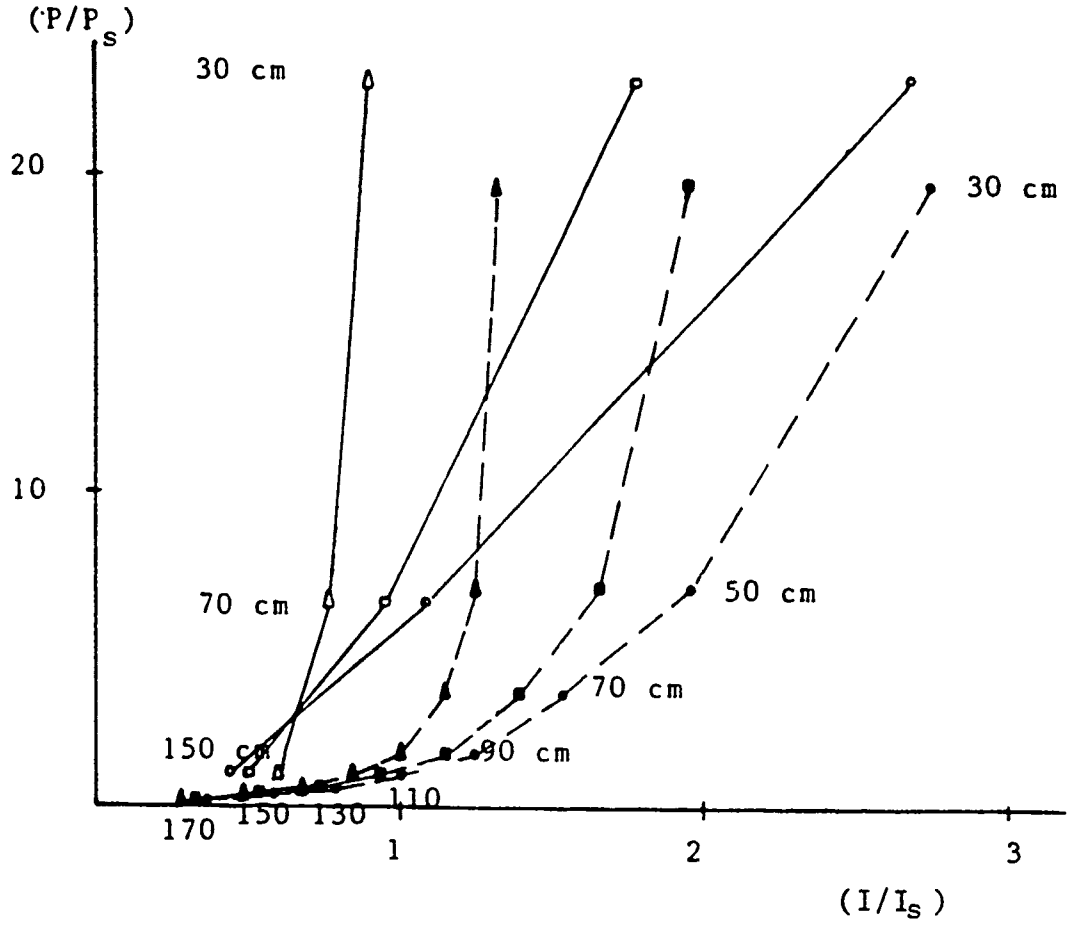

Figure 17. Comparison of Peak Stress and Impulse Between Free-Field and Three Standoff Calculations. Stress and impulse were normalized by the corresponding values of 110 cm standoff calculation, which are signified by subscript "s".

(The reverse of this page is blank.)

REFERENCES

1. Sorrell, F. Y., Horie, Y., and Whitfield, J. K., Scaling Problems for Wave Propagation in Layered Systems, ESL-TR-87-73, Vol. 1, U.S. Air Force Engineering and Services Ctr., Tyndall AFB, FL, 1988.

2. Horie, Y., Lee, S. H., and Park, J-K, Scaling Problems for Wave Propagation in Layered Systems, ESL-TR-87-73, U.S. Air Force Engineering & Service Center, Tyndall AFB, FL, 1988.

3. Chhabildas, L. C. and Graham, R. A., "Developments in Measurement Techniques for Shock-Loaded Solids," High Temperatures-High Pressures, Vol 19, 1978.

4. Chung, R. M., Bur, A. J. and Reasner, E., Development of an NBS Polymer Gage for Dynamic Soil Stress Measurement, NBSIR 85-3135, April 1985.

5. Perez, M. and Chartagnac, P. "Shock Loading and Unloading Behavior of Carbon Piezoresistive Gauges Up to 5 GPa," Rev. Sci Instrum., Vol 51, 1980.

6. Kiger, S. A. and Albritton, G. E., Response of Buried Hardened Box Structures to the Effects of Localized Explosions, U.S Army Engineer Waterways Experiment Station Technical Report SL-80-1, March 1980.

7. Baylot, J. T., Kiger, S. A., Marchand, K. A., and Painter, J. T., Response of Buried Structures to Earth Penetrating Conventional Weapons, ESL-TR-85-09, U.S. Air Force Engineering and Services Center, Tyndall AFB, FL, 1985.

8. Drake, J.L., and Little, C.D., "Ground Shock from Penetrating Conventional Weapons," Symposium on the Interaction of Non-nuclear Munitions with Structures, U.S. Air Force Academy, Colorado, May 10-13, 1983, University of Florida Graduate Engineering Center, Eglin AFB, FL, 1983.

9. Abramson, H. N., "A Broader Perspective," Second Symposium on the Interaction of Non-Nuclear Munitions with Structures, Panama City Beach, Fl, April 16-18, 1985.

10. Florence, A.L., Critical Load for Reinforced Concrete Bunkers, Final Report, DNA 001-77-C-0181, SRI International, Menlo Park, CA, 1977.

APPENDIX A

A. Loading Profiles for the Instrumented Shots

List of loading Profiles:

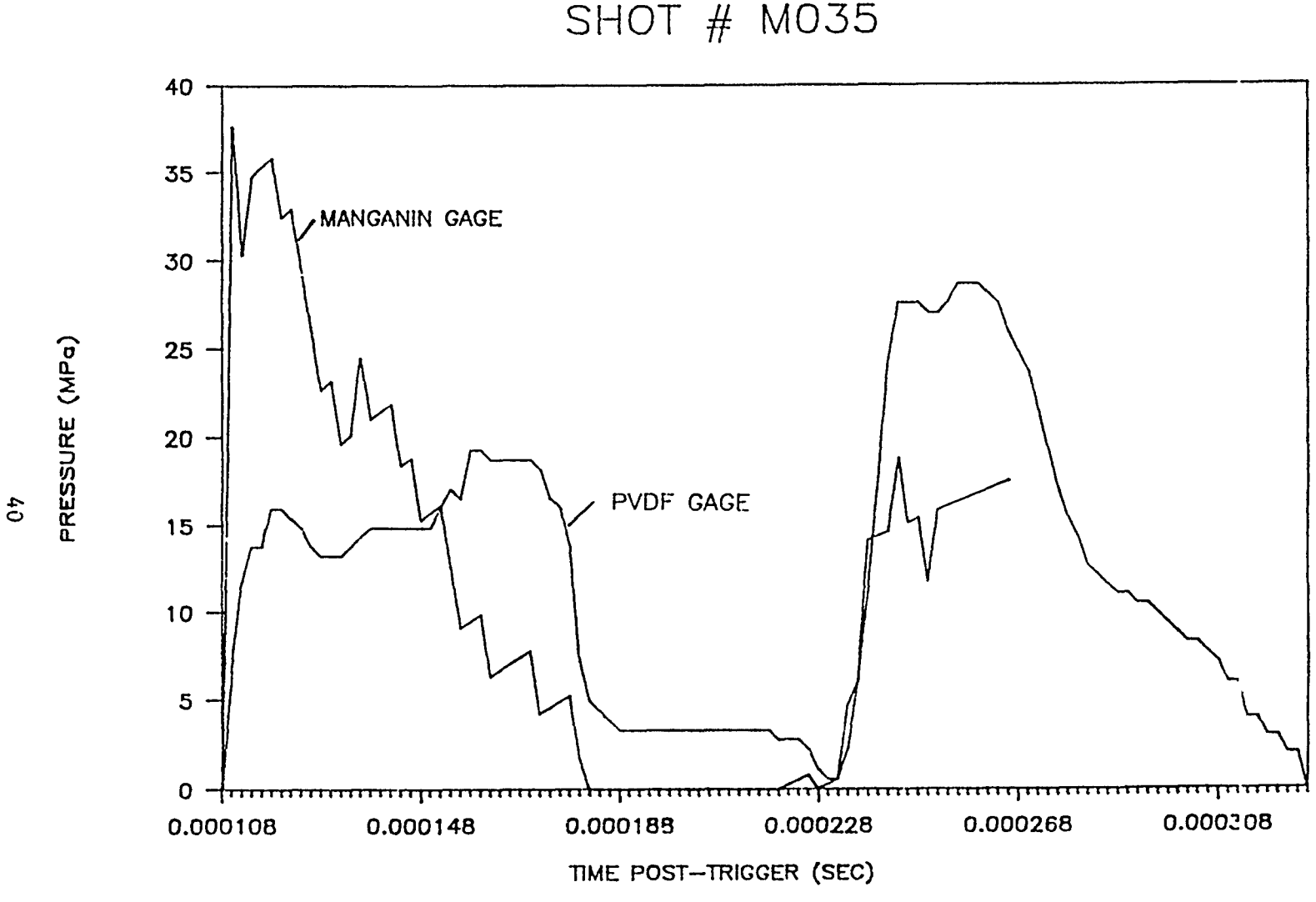

Figure A-1. Shot M035 - Manganin and PVDF Gage Output.

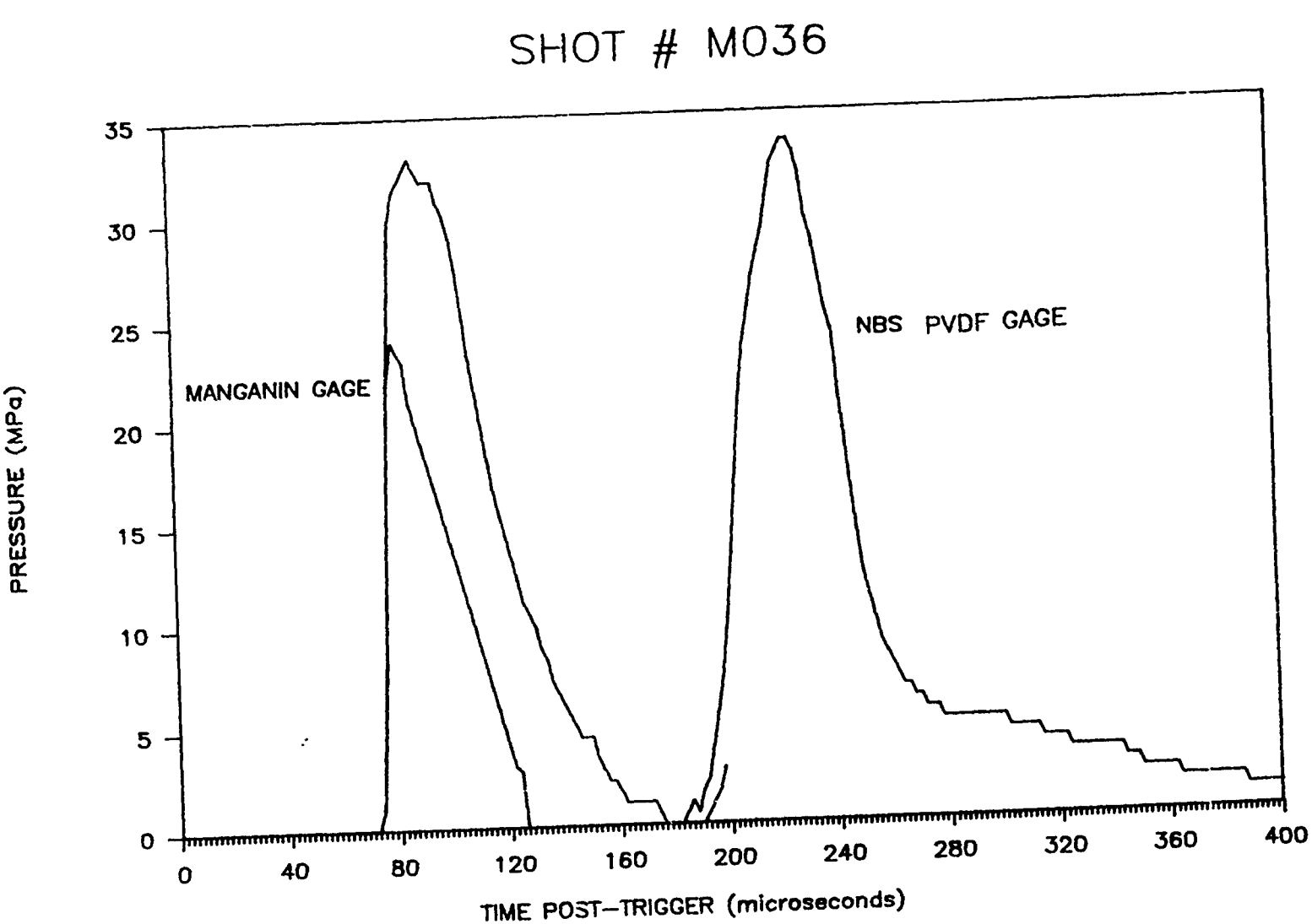

Figure A-2. Shot M036 - Manganin and PVDF Gage Output.

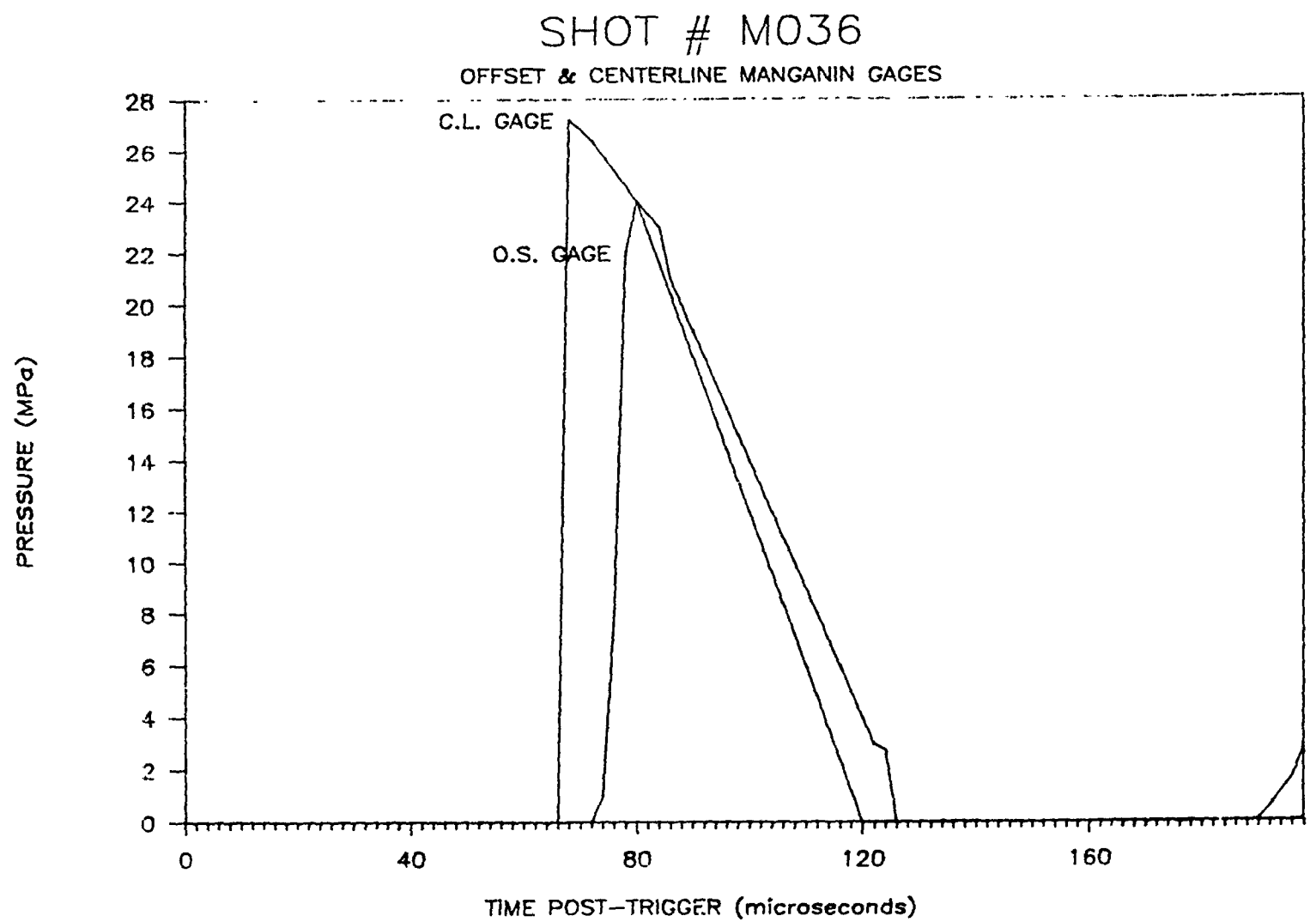

Figure A-3. Shot M036 - Centerline and Offset Manganin Gage Output.

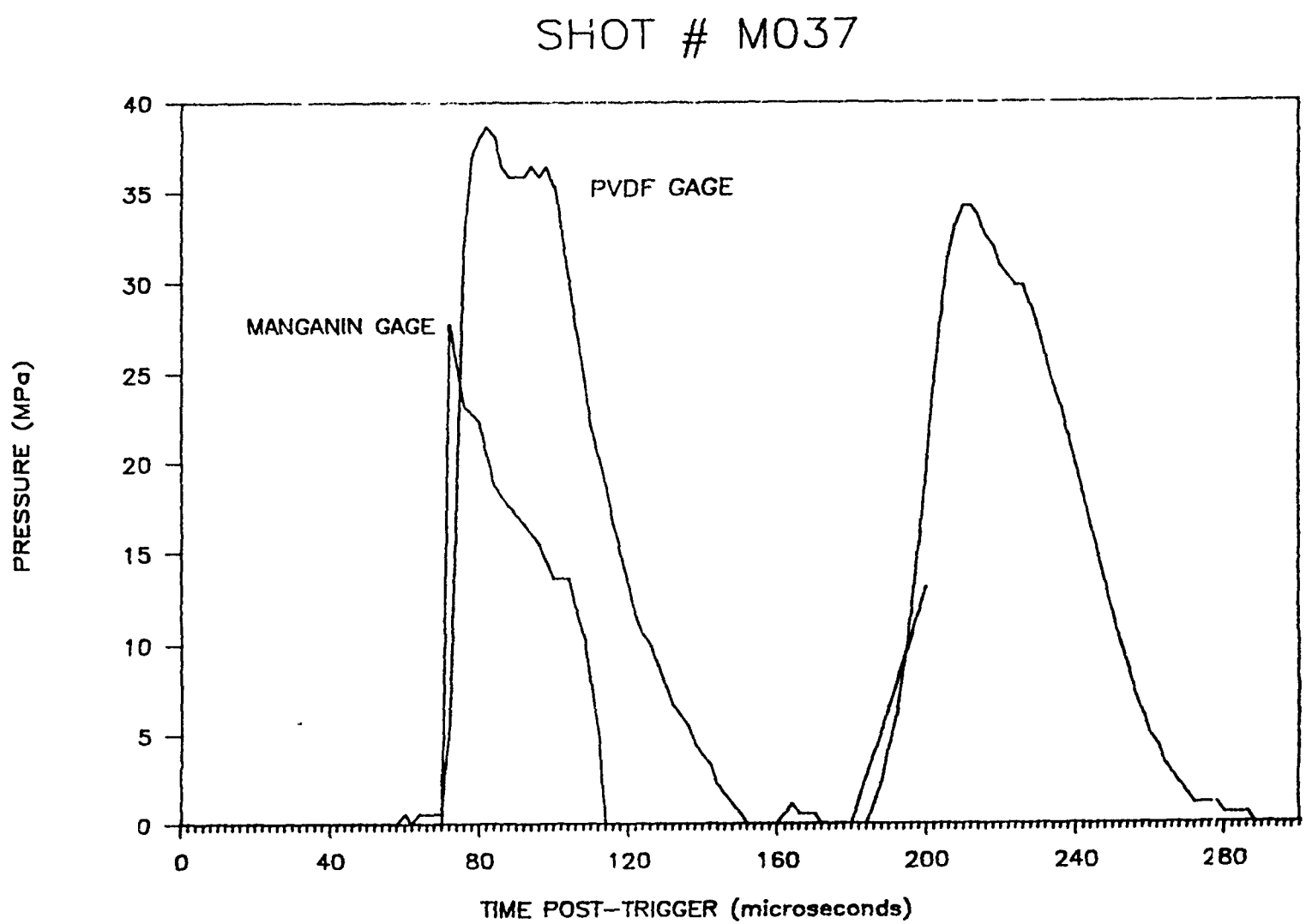

Figure A-4. Shot M037 - Manganin and PVDF Gage Output.

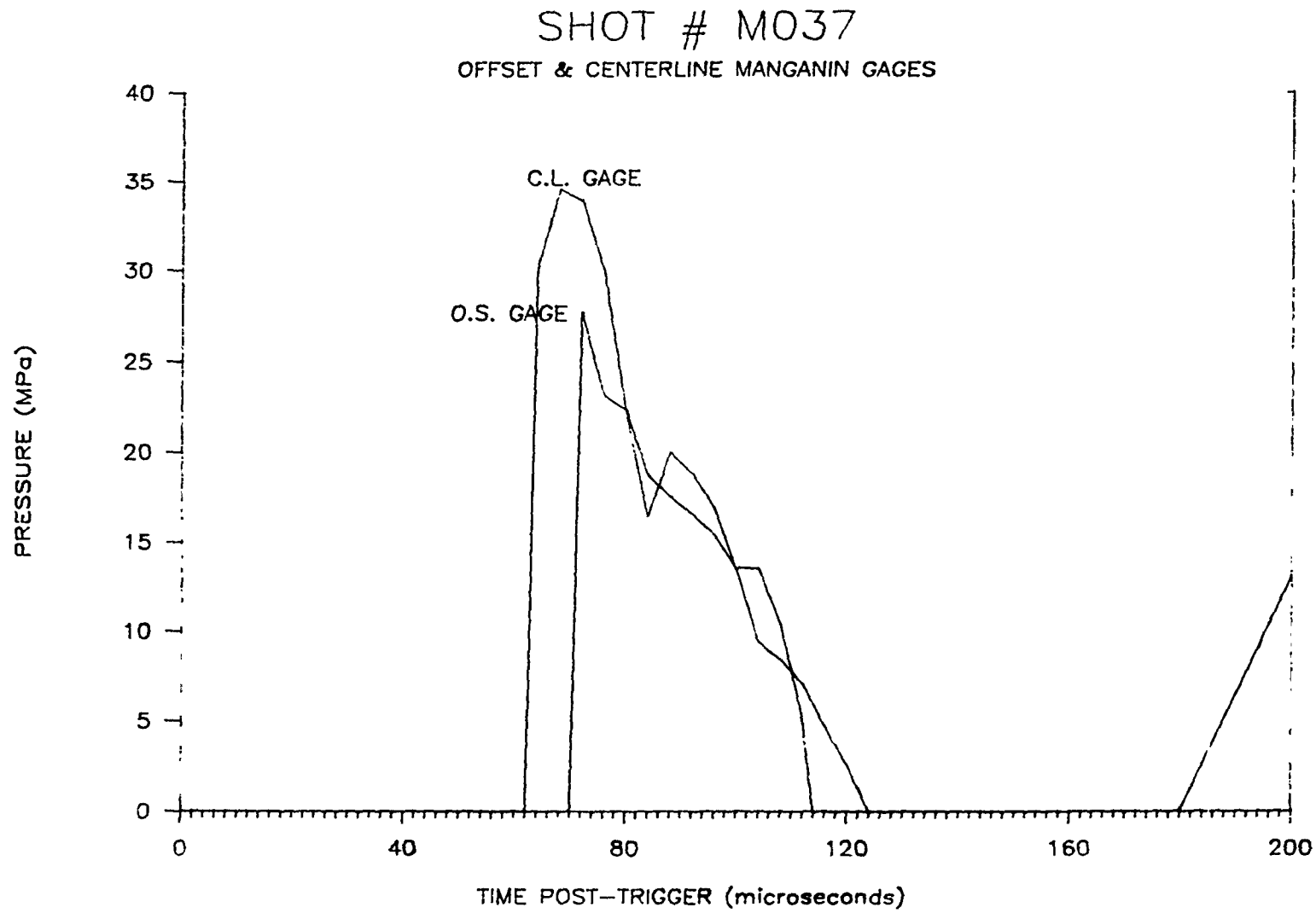

Figure A-5. Shot M037 - Centerline and Offset Manganin Gage Output.

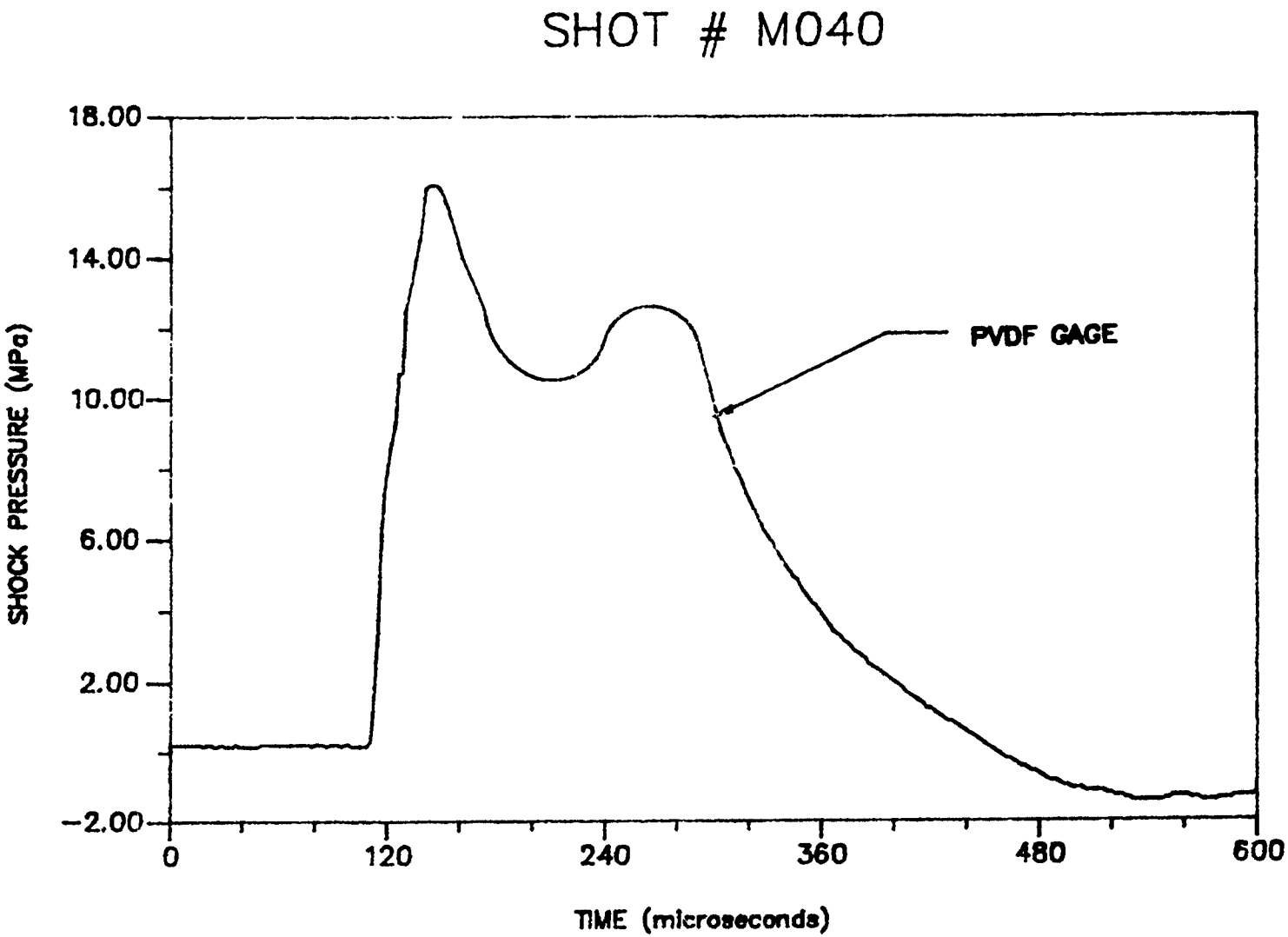

Figure A-6. Shot M040 - PVDF Gage Output.

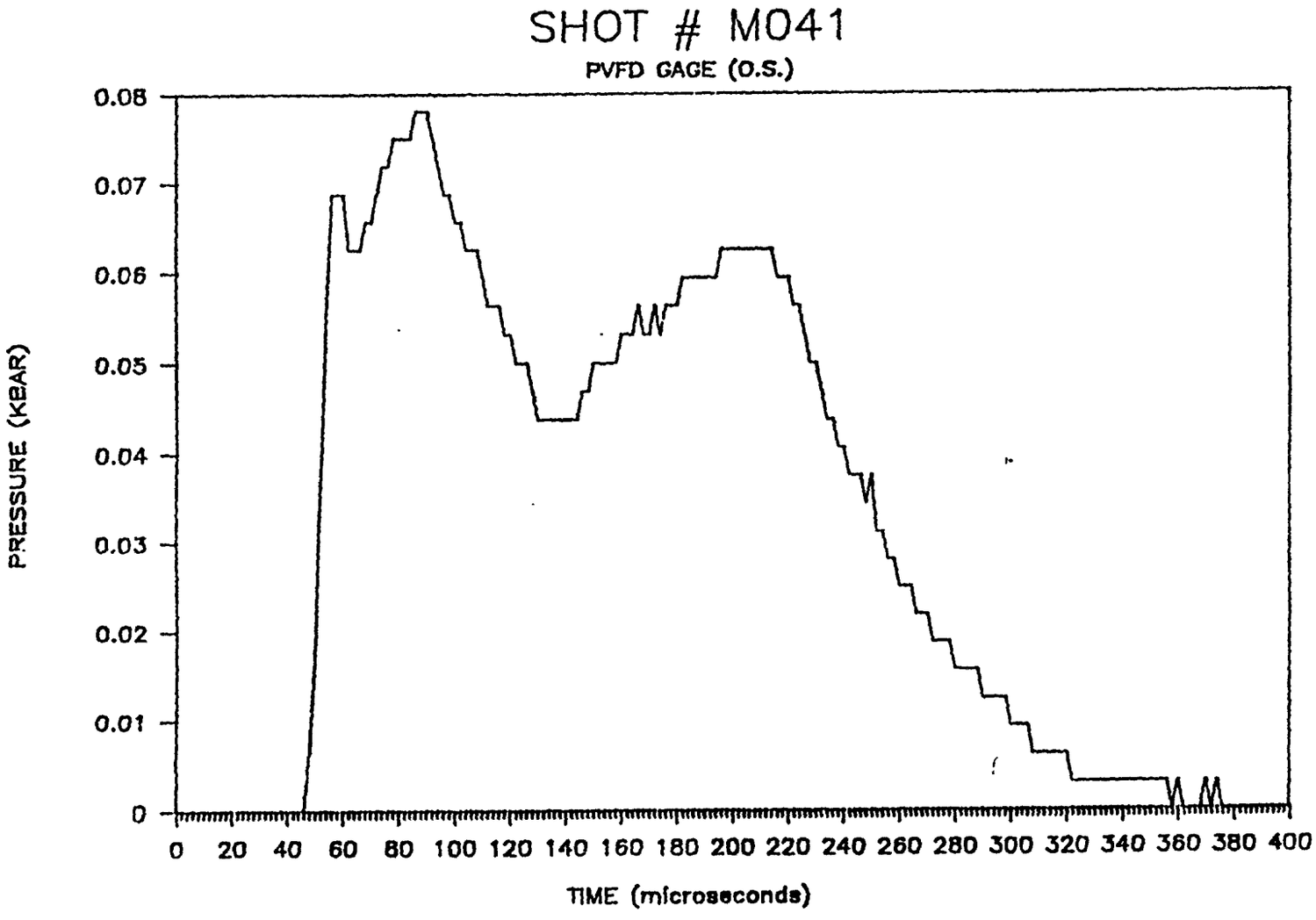

Figure A-7. Shot M041 - PVDF Gage Output.

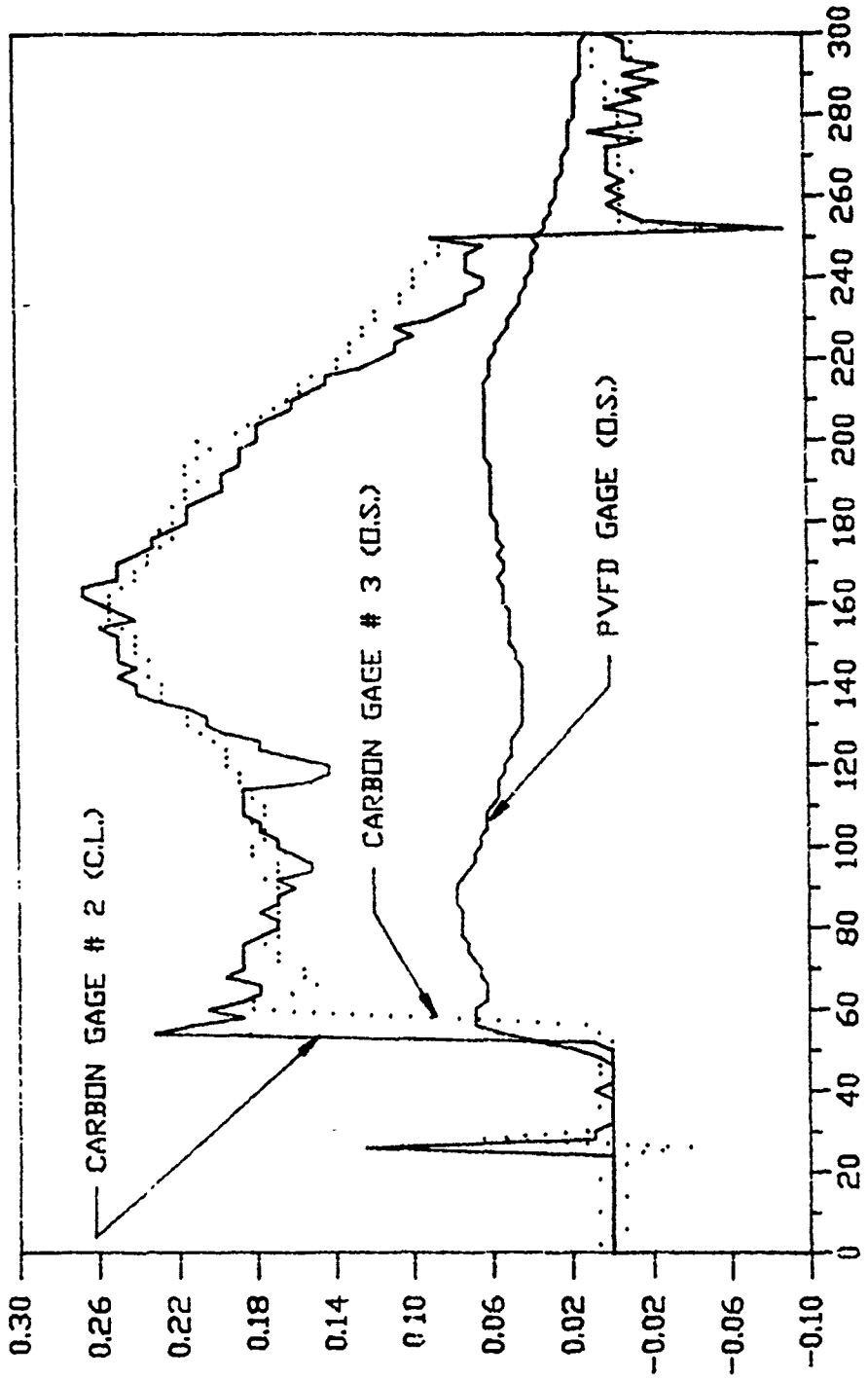

Figure A-8. Shot M041 - Centerline and Offset Carbon Gage and PVDF Gage Output.

(The reverse of this page is blank.)